

Abraham and Minkowski Poynting vector controversy in axion modified electrodynamics

Michael E Tobar,^{1,*} Ben T McAllister,¹ and Maxim Goryachev¹

¹*ARC Centre of Excellence for Engineered Quantum Systems and ARC Centre of Excellence for Dark Matter Particle Physics, Department of Physics, University of Western Australia, 35 Stirling Highway, Crawley, WA 6009, Australia.*

(Dated: March 10, 2022)

The most sensitive haloscopes that search for axion dark matter through the two photon electromagnetic anomaly, convert axions into photons through the mixing of axions with a large background DC magnetic field. In this work we apply Poynting theorem to the resulting axion modified electrodynamics and identify two possible Poynting vectors, one which is similar to the Abraham Poynting vector in electrodynamics and the other to the Minkowski Poynting vector. Inherently the conversion of axions to photons is a non-conservative process with respect to the created oscillating photonic degree of freedom. We show that Minkowski Poynting theorem picks up the added non-conservative terms while the Abraham does not. The non-conservative terms may be categorised more generally as “curl forces”, which in classical physics are non-conservative and non-dissipative forces localised in space, not describable by a scalar potential and exist outside the global conservative physical equations of motion. To understand the source of energy conversion and power flow in the detection systems, we apply the two different Poynting theorems to both the resonant cavity haloscope and the broadband low-mass axion haloscope. Our calculations show that both Poynting theorems give the same sensitivity for a resonant cavity axion haloscope, but predict markedly different sensitivity for the low-mass broadband capacitive haloscope. Hence we ask the question, can understanding which one is the correct one for axion dark matter detection, be considered under the framework of the Abraham–Minkowski controversy? In reality, this should be confirmed by experiment when the axion is detected. However, many electrodynamic experiments have ruled in favour of the Minkowski Poynting vector when considering the canonical momentum in dielectric media. In light of this, we show that the axion modified Minkowski Poynting vector should indeed be taken seriously for sensitivity calculation for low-mass axion haloscopes in the quasi static limit, and predict orders of magnitude better sensitivity than the Abraham Poynting vector equivalent.

I. Introduction

The axions is postulated to exist as a neutral spin-zero bosons to solve the strong charge-parity problem in QCD. Such a particle is predicted to couple very weakly to other known particles and has thus been postulated to be cold dark matter [1–13]. In particular, many experiments rely on the electromagnetic anomaly, which is a two photon coupling term with the axion. To gain a significant sensitivity, it is widely considered that the best way to search for the axion is when the first background photonic degrees of freedom is a large DC magnetic field, which generates a second photon that can be detected. This is the basis of the DC magnetic field axion haloscope, first proposed by Sikivie [14, 15] and pioneered experimentally by the ADMX collaboration [16–22]. Recently the scientific case that dark matter may include QCD axions or axion like particles of varied mass and photon coupling has gained momentum [23–34], leading to many new ideas and new detectors designs world-wide, which implement the principle of dark matter detection through the electromagnetic anomaly [35–75].

Inherently, the conversions of axions amongst a DC magnetic background field into a second photonic degree of freedom is a non-conservative process with respect to

the second degree of freedom. In this process, the axion mixes with the background field to create a source term that drives the energy of conversion in the second photonic degree of freedom at a frequency corresponding to the axion mass. In this work, we implement Poynting theorem to understand the source of energy conversion and flow in the system when considering axion modified electrodynamics.

In standard electrodynamics, Poynting vector analysis is implemented in circuit and antenna theory to understand how the input source power is impressed into the system along with the system power flow and how it relates to the stored energy and losses [76–80]. In this work we undertake a similar analysis within the frame work of axion modified electrodynamics. In other work, the Poynting vector has been implemented with versions of the stress-energy tensor to understand energy and forces in magnetic and dielectric matter. For example, forces in systems such as optical tweezers [81–84] and ion trapping [85], where the correct way to analyse these systems has been a subject of controversy (known as the Abraham–Minkowski controversy) and is still an active area of debate [86–92]. This debate has led to the general concept of “curl forces”, which are abundant in nature and cannot be described from the gradient of a scalar potential, and only exist in a localised space. For example, the force on a particle with complex electric polarizability is known not to be derivable from a scalar potential

* michael.tobar@uwa.edu.au

as its curl is non-zero [81, 82, 93]. Such forces are non-conservative and non-dissipative, and their inclusion has been described both classically, and quantum mechanically [94, 95], in particular the quantising of electrodynamics in dielectric and dispersive media [96]. Note, such non-conservative “curl forces” do not include the most well-known “curl force”, which is the magnetic Lorentz force, as it is a conservative force that can do no work [94], described by a magnetic vector potential.

With this in mind, it has become evident that it is possible to derive alternative versions of Poynting’s theorem (in fact four versions are possible)[97]. In particular the Minkowski Poynting vector [98], $\vec{S}_{DB} = \frac{1}{\epsilon_0 \mu_0} \vec{D} \times \vec{B}$, has been shown to be successful to account for experiments in dielectric media, where the field momentum is associated with the canonical momentum [87, 90, 92, 99], here the electric flux density, $\vec{D} = \epsilon_0 \vec{E} + \vec{P}$, is the sum of the electric field, \vec{E} , and electric polarization, \vec{P} , and the magnetic flux density, $\vec{B} = \mu_0(\vec{H} + \vec{M})$, is the sum of the magnetic field, \vec{H} and magnetization, \vec{M} . Naturally, when the the curl of the polarization is non zero ($\nabla \times \vec{P} \neq 0$) the Minkowski Poynting vector will pick up this term, due to an unconventional but necessary modification to Faraday’s law [96, 97], while the Abraham Poynting vector [100, 101], $\vec{S}_{EH} = \vec{E} \times \vec{H}$, will not. For the curl of the polarization to be non-zero, an energy input is required to seperate the bound charge, this describes a permanent electret or energy harvesting material [102] and actually describes an external non-conservative force (or fictitious force) input similar to an impressed electric field (or fictitious electric field) that drives an active dipole in antenna theory or a voltage source in circuit theory. Furthermore, the electret or energy harvester may be classified as an active bound charge dipole. We may recognise this active dipole term generally as a non-conservative “curl force”, which necessarily modifies Faraday’s law, and is only present internally to the active antenna, voltage source or electret and not present globally outside the active device. As with all “curl forces”, this non-conservative term cannot be characterised by a scalar potential, on the other hand it has been recently shown to be characterised via an electric vector potential [61, 96, 102–104].

Recently, it was also shown that there exists a similar non-conservative “curl force” term in axion modified electrodynamics [61, 104]. This occurs when the axion mixes with a DC background magnetic field, which converts the axion mass to the energy of the second photonic degree of freedom [61, 104]. In this representation the axion mixing with the DC magnetic field adds a similar term to a polarization with a non-zero curl [102, 103]. In this work we apply the Minkowski and Abraham Poynting vector equivalents to axion modified electrodynamics and compare the difference, where the former picks up the extra “curl force” term, while the latter does not.

II. The Effective Axion Current and Charge Density

It is well known that axions modify electrodynamics through the axion two photon coupling [31, 105], which in vacuum leads to the following set of modified Maxwell’s equations,

$$\begin{aligned} \nabla \cdot \vec{E} &= \frac{\rho_e}{\epsilon_0} + c g_{a\gamma\gamma} \vec{B} \cdot \nabla a \\ \nabla \times \vec{B} - \frac{1}{c^2} \partial_t \vec{E} &= \mu_0 \vec{J}_e - g_{a\gamma\gamma} \mu_0 \epsilon_0 c (\vec{B} \partial_t a + \nabla a \times \vec{E}) \\ \nabla \cdot \vec{B} &= 0 \\ \nabla \times \vec{E} + \partial_t \vec{B} &= 0 \end{aligned} \quad (1)$$

Here $g_{a\gamma\gamma}$ is the two-photon coupling to an axion field, $a(t)$ is the amplitude of the axion field, ρ_e is the volume charge density and \vec{J}_e the volume current density. One common way to set up the equations of motion for the two photon interaction is to assume $\nabla a = 0$, so two of the three terms go to zero and only one modification to Ampere’s law remains,

$$\nabla \times \vec{B} - \frac{1}{c^2} \partial_t \vec{E} = \mu_0 (\vec{J}_e - g_{a\gamma\gamma} \epsilon_0 c \vec{B} \partial_t a), \quad (2)$$

where the axion current is defined by,

$$\vec{J}_a = -g_{a\gamma\gamma} \epsilon_0 c \vec{B} \partial_t a. \quad (3)$$

This modification is commonly used in the calculation of sensitivity of haloscope experiments.

A more general version of the modifications as source terms can be obtained by substituting the following vector identities, $\vec{B} \cdot \nabla a = \nabla \cdot (a \vec{B}) - a (\nabla \cdot \vec{B})$ and $\nabla a \times \vec{E} = \nabla \times (a \vec{E}) - a (\nabla \times \vec{E})$ into (1). Then, assuming to first order $\nabla \cdot \vec{B} = 0$ and $\nabla \times \vec{E} = -\partial_t \vec{B}$, the modified Gauss’ and Ampere’s Laws, may be written as [31, 104],

$$\begin{aligned} \epsilon_0 \nabla \cdot \vec{E} &= \rho_e + \rho_{ab} \\ \frac{1}{\mu_0} \nabla \times \vec{B} - \epsilon_0 \partial_t \vec{E} &= \vec{J}_e + \vec{J}_{ab} + \vec{J}_{ae}, \end{aligned} \quad (4)$$

where

$$\begin{aligned} \rho_{ab} &= g_{a\gamma\gamma} \epsilon_0 c \nabla \cdot (a(t) \vec{B}(\vec{r}, t)) \\ \vec{J}_{ab} &= -g_{a\gamma\gamma} \epsilon_0 c \partial_t (a(t) \vec{B}(\vec{r}, t)) \\ \vec{J}_{ae} &= -g_{a\gamma\gamma} \epsilon_0 c \nabla \times (a(t) \vec{E}(\vec{r}, t)) \end{aligned} \quad (5)$$

Here, \vec{J}_{ab} is similar to a polarisation current, and ρ_{ab} is similar to a bound charge, and are related through the continuity equation,

$$\nabla \cdot \vec{J}_{ab} = -\partial_t \rho_{ab}. \quad (6)$$

Furthermore, \vec{J}_{ae} is similar to a bound current, so the total axion current is thus $\vec{J}_a = \vec{J}_{ab} + \vec{J}_{ae}$, which is a more

general form of Eqn. (3). Note, that setting these terms to zero because $\nabla a = 0$, at the begining of a calculation that analyses the sensitivity of a axion-photon coupled system can result in missing some parts of the solution [61, 104], as we show in the next section.

III. Axion Modified Electrodynamics

A. Time Dependent Form

Rather than write the equation of motion with modified source terms, as in (4) and (5), we may include the modifications in the definitions of the fields themselves in a similar way to the auxiliary fields in matter [104]. With some rearrangement of these equations, we can show [31, 102, 106],

$$\begin{aligned} \nabla \cdot (\vec{E}(\vec{r}, t) - g_{a\gamma\gamma}a(t)c\vec{B}(\vec{r}, t)) &= \frac{\rho_e}{\epsilon_0} \\ \nabla \times (c\vec{B}(\vec{r}, t) + g_{a\gamma\gamma}a(t)\vec{E}(\vec{r}, t)) \\ - \frac{1}{c}\partial_t(\vec{E}(\vec{r}, t) - g_{a\gamma\gamma}a(\vec{r}, t)c\vec{B}(\vec{r}, t)) &= c\mu_0\vec{J}_e \quad (7) \\ \nabla \cdot c\vec{B}(\vec{r}, t) &= 0 \\ \nabla \times \vec{E}(\vec{r}, t) + \frac{1}{c}\partial_t c\vec{B}(\vec{r}, t) &= 0. \end{aligned}$$

This has been shown to be equivalent to a pertubative transformation of the electromagnetic fields [104, 107, 108], given by,

$$c\vec{B}'(\vec{r}, t) \rightarrow c\vec{B}(\vec{r}, t) + g_{a\gamma\gamma}a(t)\vec{E}(\vec{r}, t), \quad \text{and} \quad (8)$$

$$\vec{E}'(\vec{r}, t) \rightarrow \vec{E}(\vec{r}, t) - g_{a\gamma\gamma}a(t)c\vec{B}(\vec{r}, t). \quad (9)$$

Where equations (8) and (9) in the quasi-static limit, effectively represent dual symmetry with respect to a rotation angle, $\theta(t) = g_{a\gamma\gamma}a(t)$ where $\theta(t) \ll 1$ [109–112]. Here $\theta(t)$ is an effective dynamical pseudo-scalar field, which in this case is the product of the axion pseudo-scalar field, $a(t)$, with the axion photon coupling, $g_{a\gamma\gamma}$. For dark matter axions, $a(t)$ is in general a large classical field, however $\theta(t)$ remains small due to the extremely weak coupling of axions to photons, i.e. $g_{a\gamma\gamma} \ll 1$. Note, there is also a duality transformation between electromagnetic potentials, where the dual 4-vector potential contains a magnetic scalar potential and an electric vector potential. Under this duality transform the electric vector potential manifests [108–112], which potentially adds the axion induced “curl force” to the system under investigation. This is evident from eqn. (9), as the curl of \vec{E}' has a non-zero spatial term.

Now considering the interaction includes two photons, we distinguish between a background field (denoted by subscript 0) and the generated photon field (denoted by subscript 1), which is created by the axion pseudo-scalar field mixing with the background field. To first order we may assume the background field satisfies Maxwell's

equations, so that,

$$\begin{aligned} \nabla \times \vec{B}_0 &= \mu_0\epsilon_0\partial_t\vec{E}_0 + \mu_0\vec{J}_{e_0} \\ \nabla \times \vec{E}_0 &= -\partial_t\vec{B}_0 \\ \nabla \cdot \vec{B}_0 &= 0 \\ \nabla \cdot \vec{E}_0 &= \epsilon_0^{-1}\rho_{e_0} \end{aligned} \quad (10)$$

Note, any axion modification of the back ground field will end up second order with respect to the effects on the second generated photonic degree of freedom, so can be ignored[31, 106].

Thus for the generated photonic degree of freedom, we may write (7) in a similar way to how the auxiliary fields are included in Maxwell's equations in matter, and we find axion modified electrodynamics in familiar form[104], given by,

$$\begin{aligned} \nabla \cdot \vec{D}_1 &= \rho_{e1} \\ \nabla \times \vec{H}_1 - \partial_t\vec{D}_1 &= \vec{J}_{e1} \\ \nabla \cdot \vec{B}_1(\vec{r}, t) &= 0 \\ \nabla \times \vec{E}_1(\vec{r}, t) + \partial_t\vec{B}_1(\vec{r}, t) &= 0, \end{aligned} \quad (11)$$

where (8) and (9) are akin to the following constitutive relations,

$$\begin{aligned} \vec{H}_1(\vec{r}, t) &= \frac{\vec{B}_1}{\mu_0} - \vec{M}_1 - \vec{M}_{1a}, \quad \text{and} \\ \vec{D}_1(\vec{r}, t) &= \epsilon_0\vec{E}_1 + \vec{P}_1 + \vec{P}_{1a}. \end{aligned} \quad (12)$$

Here, \vec{M}_1 and \vec{P}_1 are the non axion induced magnetization and polarization respectively, while the axion modifications, \vec{M}_{1a} and \vec{P}_{1a} are moved to redefinitions of the auxiliary fields rather than source terms, and to first order with respect to the background field are given by,

$$\begin{aligned} \vec{M}_{1a} &= -g_{a\gamma\gamma}a(t)c\epsilon_0\vec{E}_0(\vec{r}, t) \quad \text{and} \\ \frac{1}{\epsilon_0}\vec{P}_{1a} &= -g_{a\gamma\gamma}a(t)c\vec{B}_0(\vec{r}, t), \end{aligned} \quad (13)$$

Here it is clear the the divergence of \vec{M}_{1a} is non-zero, similar to what occurs at the boundaries of a permanent magnet, and the curl of \vec{P}_{1a} is non zero similar to what occurs at the boundaries of a permanent electret, and by combining (13) and (10) can be calculated to be (assuming $\nabla a = 0$),

$$\begin{aligned} \nabla \cdot \vec{M}_{1a} &= -g_{a\gamma\gamma}a(t)c\epsilon_0\nabla \cdot \vec{E}_0(\vec{r}, t) = -g_{a\gamma\gamma}a(t)c\rho_{e_0} \\ \frac{1}{\epsilon_0}\nabla \times \vec{P}_{1a} &= -g_{a\gamma\gamma}a(t)c\nabla \times \vec{B}_0(\vec{r}, t) \\ &= -\frac{g_{a\gamma\gamma}a(t)}{c}\partial_t\vec{E}_0 - g_{a\gamma\gamma}a(t)c\mu_0\vec{J}_{e_0}. \end{aligned} \quad (14)$$

Note, if we followed the procedure to set $\nabla a = 0$ at the start of the calculation, then the axion current in (3) would be the only modification, and the general form

of the modified constitutive relations in (12) would be missed. This would be akin to falsely setting $\nabla \times \vec{P}_{a1} = 0$ and $\nabla \cdot \vec{M}_{a1} = 0$ even though they are in general non-zero in the approximation when ∇a is set to zero.

Assuming only a DC background magnetic field, $\vec{B}_0(\vec{r})$ with no background electric field ($\vec{E}_0 = 0$ and $\vec{M}_{a1} = 0$) and in vacuum ($\vec{M}_1 = 0$, $\vec{P}_1 = 0$ and $\vec{B}_1 = \mu_0 \vec{H}_1$), one can write the axion modified Ampere's and law from eqn. (11) as,

$$\nabla \times \vec{B}_1 = \mu_0 \partial_t \vec{D}_1 + \mu_0 \vec{J}_{e1} \quad (15)$$

In contrast, Faraday's law with respect to the \vec{E}_1 and \vec{B}_1 fields remains unchanged,

$$\nabla \times \vec{E}_1 = -\partial_t \vec{B}_1. \quad (16)$$

However, given the fact that the curl of \vec{P}_{a1} in eqn. (14) is non-zero, a modified Faraday's law may be written in a similar fashion as to what is undertaken with an electret or impressed voltage source when the curl is non-zero [96, 97, 102], so by taking the curl of \vec{D}_1 in (12) and combining with (16) we obtain,

$$\frac{1}{\epsilon_0} \nabla \times \vec{D}_1 = -\partial_t \vec{B}_1 - g_{a\gamma\gamma} a \mu_0 c \vec{J}_{e0}, \quad (17)$$

which is analogous to an electromagnetic systems in matter where the curl of the polarization is non-zero. It has been shown in such systems the fundamental electromagnetic quantities become the electric \vec{D} and magnetic \vec{B} flux densities [96, 97, 102], which is compatible with the Minkowski Poynting vector.

In this work we apply these more general equations to low-mass axion haloscopes, which necessarily include the impressed current, \vec{J}_{e0} , which creates the background magnetic field $\vec{B}_0(\vec{r})$. Note, there also exist a dual symmetry with the source terms in the above equation (15) and (17), where an effective impressed magnetic current manifests through the axion interaction with the impressed electrical current, \vec{J}_{e0} , so $\vec{J}'_{m1}(\vec{r}, t) \rightarrow g_{a\gamma\gamma} a(t) \mu_0 c \vec{J}_{e0}(\vec{r}, t)$. The fact that this impressed magnetic current exists, does not necessitate the existence of free magnetic monopoles, in the same way bound currents and polarization currents do not need the existence of free electrons or any other free charge carrier. For example, bound magnetic monopoles exist in nature as permanent magnets consisting of bound north and south pole pairs, which can be set in motion, with a net bound magnetic current if one pole is kept stationary as the other rotates. Such a rotating magnet converts the mechanical motion to an electromotive force with non-zero curl (a curl force) [102]. This fact has been recognised as early as 1936 [113], where Schelkunoff from Bell Labs stated "It is true that there are no magnetic conductors and no magnetic conduction currents in the same sense as there are electric conductors and electric conduction currents but magnetic convection currents are just as real

as electric convection currents, although the former exist only in doublets of oppositely directed currents since magnetic charges themselves are observable only in doublets."

B. Harmonic Phasor Form

For harmonic solutions of the axion-Maxwell equations we write the equations in complex vector-phasor form. For example, we set $\vec{E}_1(\vec{r}, t) = \frac{1}{2} (\mathbf{E}_1(\vec{r}) e^{-j\omega_1 t} + \mathbf{E}_1^*(\vec{r}) e^{j\omega_1 t}) = \text{Re} [\mathbf{E}_1(\vec{r}) e^{-j\omega_1 t}]$, so we define the vector phasor (bold) and its complex conjugate by, $\tilde{\mathbf{E}}_1(\vec{r}, t) = \mathbf{E}_1(\vec{r}) e^{-j\omega_1 t}$ and $\tilde{\mathbf{E}}_1^*(\vec{r}, t) = \mathbf{E}_1^*(\vec{r}) e^{j\omega_1 t}$, respectively. In contrast, the axion pseudo-scalar field, $a(t)$, may be written as, $a(t) = \frac{1}{2} (\tilde{a} e^{-j\omega_a t} + \tilde{a}^* e^{j\omega_a t}) = \text{Re} (\tilde{a} e^{-j\omega_a t})$, and thus, in phasor form, $\tilde{A} = \tilde{a} e^{-j\omega_a t}$ and $\tilde{A}^* = \tilde{a}^* e^{j\omega_a t}$. Thus, the phasor form of the modified Ampere's law in (15) becomes,

$$\begin{aligned} \frac{1}{\mu_0} \nabla \times \tilde{\mathbf{B}}_1 &= \tilde{\mathbf{J}}_{e1} - j\omega_1 \epsilon_0 \tilde{\mathbf{E}}_1 + j\omega_a g_{a\gamma\gamma} \epsilon_0 c \tilde{A} \vec{B}_0 \\ \frac{1}{\mu_0} \nabla \times \tilde{\mathbf{B}}_1^* &= \tilde{\mathbf{J}}_{e1}^* + j\omega_1 \epsilon_0 \tilde{\mathbf{E}}_1^* - j\omega_a g_{a\gamma\gamma} \epsilon_0 c \tilde{A}^* \vec{B}_0, \end{aligned} \quad (18)$$

while, the phasor form of the Faraday's law in (16) becomes,

$$\begin{aligned} \nabla \times \tilde{\mathbf{E}}_1 &= j\omega_1 \times \tilde{\mathbf{B}}_1 \\ \nabla \times \tilde{\mathbf{E}}_1^* &= -j\omega_1 \times \tilde{\mathbf{B}}_1^*, \end{aligned} \quad (19)$$

and the phasor form of the modified Faraday's law in (17) becomes,

$$\begin{aligned} \frac{1}{\epsilon_0} \nabla \times \tilde{\mathbf{D}}_1 &= j\omega_1 \tilde{\mathbf{B}}_1 - g_{a\gamma\gamma} c \mu_0 \tilde{A} \vec{J}_{e0} \\ \frac{1}{\epsilon_0} \nabla \times \tilde{\mathbf{D}}_1^* &= -j\omega_1 \tilde{\mathbf{B}}_1^* - g_{a\gamma\gamma} c \mu_0 \tilde{A}^* \vec{J}_{e0} \end{aligned} \quad (20)$$

In the following we use these equations to calculate energy and power via Poynting theorem in a DC magnetic field axion haloscope.

IV. Calculation of Power Generated in a DC Magnetic Field Axion Haloscope using Poynting Theorem

We start by considering the instantaneous Poynting vector in its standard physics text book form of,

$$\begin{aligned} \vec{S}_1(t) &= \frac{1}{\mu_0} \vec{E}_1(t) \times \vec{B}_1(t) = \\ &\frac{1}{2} (\mathbf{E}_1 e^{-j\omega_1 t} + \mathbf{E}_1^* e^{j\omega_1 t}) \times \frac{1}{2\mu_0} (\mathbf{B}_1 e^{-j\omega_1 t} + \mathbf{B}_1^* e^{j\omega_1 t}) \\ &= \frac{1}{2\mu_0} \text{Re} (\mathbf{E}_1 \times \mathbf{B}_1^*) + \frac{1}{2\mu_0} \text{Re} (\mathbf{E}_1 \times \mathbf{B}_1 e^{-j2\omega_1 t}), \end{aligned} \quad (21)$$

which consists of a DC term, the first term on the right hand side of (21) and a high frequency term, the second term on the right hand side of (21). Note, the DC term in (21) is equivalent to the time average of the instantaneous Poynting vector.

Thus, the complex Poynting vector and its complex conjugate are defined by,

$$\mathbf{S}_1 = \frac{1}{2\mu_0} \mathbf{E}_1 \times \mathbf{B}_1^* \quad \text{and} \quad \mathbf{S}_1^* = \frac{1}{2\mu_0} \mathbf{E}_1^* \times \mathbf{B}_1, \quad (22)$$

respectively, where \mathbf{S}_1 is the complex power density of the harmonic electromagnetic wave or oscillation, with the real part equal to the time averaged power density and the imaginary term equal to the reactive power, which may be inductive (magnetic energy dominates) or capacitive (electrical energy dominates).

In the case that the complex Poynting vector is only real, then the \mathbf{E}_1 and \mathbf{B}_1 fields are in-phase, this describes a propagating wave with distinct direction and momentum. Such a propagating wave can be generated by an antenna in the far-field limit, at distances larger than the wavelength of the emitted photon, and is a source of loss from the antenna. Another case where \mathbf{E}_1 and \mathbf{B}_1 are in phase is due to resistive losses, in this case the photon energy is converted to heat and destroyed, however both are effectively loss terms with respect to the antenna, the former known as radiation loss. Conversely, in the near field limit of an antenna, the Poynting vector is imaginary as \mathbf{E}_1 and \mathbf{B}_1 are out of phase. This represents reactive energy flow between the antenna power source and the antenna near field, which exists at sub wavelength distances from the antenna. In this case the photons do not propagate away from the antenna, and exist as quasi-static oscillating \mathbf{E}_1 and \mathbf{B}_1 fields with no net momentum.

A convenient and unambiguous way to calculate the real and imaginary part of the Poynting vector is through the following equations,

$$\text{Re}(\mathbf{S}_1) = \frac{1}{2}(\mathbf{S}_1 + \mathbf{S}_1^*) \quad \text{and} \quad j \text{Im}(\mathbf{S}_1) = \frac{1}{2}(\mathbf{S}_1 - \mathbf{S}_1^*). \quad (23)$$

We use these equations in the following to calculate the real and imaginary part of the complex Poynting vector in axion modified electrodynamics.

A. Axion Modified Minkowski Poynting Theorem

Based on the axion modified \vec{D}_1 vector, we may calculate the complex axion modified Minkowski Poynting vector in a similar way to eqn. (22), which is given by,

$$\mathbf{S}_{DB} = \frac{1}{2\epsilon_0\mu_0} \mathbf{D}_1 \times \mathbf{B}_1^* \quad \text{and} \quad \mathbf{S}_{DB}^* = \frac{1}{2\epsilon_0\mu_0} \mathbf{D}_1^* \times \mathbf{B}_1 \quad (24)$$

Taking the divergence of eqn. (24) we find

$$\nabla \cdot \mathbf{S}_{DB} = \frac{1}{2} \nabla \cdot \left(\frac{1}{\epsilon_0} \mathbf{D}_1 \times \frac{1}{\mu_0} \mathbf{B}_1^* \right) = \frac{1}{2} \left(\frac{1}{\mu_0} \mathbf{B}_1^* \cdot \frac{1}{\epsilon_0} \nabla \times \mathbf{D}_1 - \frac{1}{\epsilon_0} \mathbf{D}_1 \cdot \frac{1}{\mu_0} \nabla \times \mathbf{B}_1^* \right), \quad (25)$$

and

$$\begin{aligned} \nabla \cdot \mathbf{S}_{DB}^* &= \frac{1}{2} \nabla \cdot \left(\frac{1}{\epsilon_0} \mathbf{D}_1^* \times \frac{1}{\mu_0} \mathbf{B}_1 \right) = \\ &\quad \frac{1}{2} \left(\frac{1}{\mu_0} \mathbf{B}_1 \cdot \frac{1}{\epsilon_0} \nabla \times \mathbf{D}_1^* - \frac{1}{\epsilon_0} \mathbf{D}_1^* \cdot \frac{1}{\mu_0} \nabla \times \mathbf{B}_1 \right). \end{aligned} \quad (26)$$

Combining (25) and (26) with (20), (18) and (23) along with the divergence theorem (this is a standard technique in microwave engineering and circuit theory [78, 97, 114, 115]), after some calculation we obtain (see Appendix A for details),

$$\begin{aligned} \oint \text{Re}(\mathbf{S}_{DB}) \cdot \hat{n} ds &= \\ \int \left(\frac{j(\omega_1 - \omega_a)}{4} \epsilon_0 g_{a\gamma\gamma} c \vec{B}_0 \cdot (\tilde{a} \mathbf{E}_1^* - \tilde{a}^* \mathbf{E}_1) \right. &+ \frac{1}{4} g_{a\gamma\gamma} c \vec{B}_0 \cdot (\tilde{a} \mathbf{J}_{e_1}^* + \tilde{a}^* \mathbf{J}_{e_1}) - \frac{1}{4} g_{a\gamma\gamma} \vec{J}_{e_0} \cdot (\tilde{a}^* c \mathbf{B}_1 + \tilde{a} c \mathbf{B}_1^*) \\ \left. - \frac{1}{4} (\mathbf{E}_1 \cdot \mathbf{J}_{e_1}^* + \mathbf{E}_1^* \cdot \mathbf{J}_{e_1}) \right) dV, & \end{aligned} \quad (27)$$

and

$$\begin{aligned} \oint j \text{Im}(\mathbf{S}_{DB}) \cdot \hat{n} ds &= \int \left(\frac{j\omega_1}{2} \left(\frac{1}{\mu_0} \mathbf{B}_1^* \cdot \mathbf{B}_1 - \epsilon_0 \mathbf{E}_1 \cdot \mathbf{E}_1^* \right) \right. &+ \frac{j(\omega_1 + \omega_a) \epsilon_0 g_{a\gamma\gamma}}{4} c \vec{B}_0 \cdot (\tilde{a} \mathbf{E}_1^* + \tilde{a}^* \mathbf{E}_1) + \\ \left. \frac{1}{4} g_{a\gamma\gamma} c \vec{B}_0 \cdot (\tilde{a} \mathbf{J}_{e_1}^* - \tilde{a}^* \mathbf{J}_{e_1}) + \frac{1}{4} g_{a\gamma\gamma} \vec{J}_{e_0} \cdot (\tilde{a}^* c \mathbf{B}_1 - \tilde{a} c \mathbf{B}_1^*) \right. \\ \left. - \frac{1}{4} (\mathbf{E}_1 \cdot \mathbf{J}_{e_1}^* - \mathbf{E}_1^* \cdot \mathbf{J}_{e_1}) \right) dV & \end{aligned} \quad (28)$$

The closed surface integral on the left hand side of (27) is the time averaged power radiated from inside to outside the haloscope volume, which for a closed system like a cavity will be zero. However, for an open system like a radio frequency antenna, real power will radiate in the far field. In contrast, the closed surface integral on the left hand side of (28) is the reactive power radiated outside the haloscope volume, which in general does not have to be zero, in a similar way to how reactive power oscillates to and from the voltage source charging and discharging a reactive capacitor in circuit theory, or the reactive power in an antenna, where energy oscillates from the antenna to the near field and then is reabsorbed by the antenna, due to the antenna's self capacitance or inductance.

B. Axion Modified Abraham Poynting Theorem

The complex Abraham pointing vector is basically the same as eqn. (22), for the case we are considering, with $\vec{H}_1 = \frac{1}{\mu_0} \vec{B}_1$. Taking the divergence of eqn. (22) we find,

$$\begin{aligned} \nabla \cdot \mathbf{S}_{EH} &= \frac{1}{2} \nabla \cdot (\mathbf{E}_1 \times \mathbf{H}_1^*) = \\ \frac{1}{2} \mathbf{H}_1^* \cdot (\nabla \times \mathbf{E}_1) - \frac{1}{2} \mathbf{E}_1 \cdot (\nabla \times \mathbf{H}_1^*) & \end{aligned} \quad (29)$$

and

$$\begin{aligned}\nabla \cdot \mathbf{S}_{EH}^* &= \frac{1}{2} \nabla \cdot (\mathbf{E}_1^* \times \mathbf{H}_1) = \\ &\frac{1}{2} \mathbf{H}_1 \cdot (\nabla \times \mathbf{E}_1^*) - \frac{1}{2} \mathbf{E}_1^* \cdot (\nabla \times \mathbf{H}_1)\end{aligned}\quad (30)$$

Combining (29) and (30) with (19), (18) and (23) along with the divergence theorem, we obtain (see Appendix A for details),

$$\oint \text{Re}(\mathbf{S}_{EH}) \cdot \hat{n} ds = \int \left(\frac{j\omega_a}{4} \epsilon_0 g_{a\gamma\gamma} c \vec{B}_0 \cdot (\tilde{a}^* \mathbf{E}_1 - \tilde{a} \mathbf{E}_1^*) \right. \\ \left. - \frac{1}{4} (\mathbf{E}_1 \cdot \mathbf{J}_{e1}^* + \mathbf{E}_1^* \cdot \mathbf{J}_{e1}) \right) dV \quad (31)$$

and

$$\oint j \text{Im}(\mathbf{S}_{EH}) \cdot \hat{n} ds = \int \left(\frac{j\omega_1}{2} (\mu_0 \mathbf{H}_1^* \cdot \mathbf{H}_1 - \epsilon_0 \mathbf{E}_1 \cdot \mathbf{E}_1^*) \right. \\ \left. + \frac{j\omega_a}{4} \epsilon_0 g_{a\gamma\gamma} c \vec{B}_0 \cdot (\tilde{a}^* \mathbf{E}_1 + \tilde{a} \mathbf{E}_1^*) \right. \\ \left. - \frac{1}{4} (\mathbf{E}_1 \cdot \mathbf{J}_{e1}^* - \mathbf{E}_1^* \cdot \mathbf{J}_{e1}) \right) dV \quad (32)$$

Like before, the closed surface integral on the left hand side of (31) and (32) is the time averaged power and reactive power radiated outside the haloscope volume respectively. However the Abraham Poynting vector misses three extra terms the Minkowski Poynting vector picks up, due to the inclusion of the non-conservative and non-dissipative source term described by eqn. (20).

C. Abraham or Minkowski Poynting Theorem in Axion Modified Electrodynamics?

Currently most calculations of haloscope detection sensitivity a priori assume the Abraham Poynting vector is valid, with the exception of one or two [61, 104]. However, as shown in the Minkowski-Abraham debate over the past century, this is not “clear-cut” and in a stationary dielectric media where the canonical momentum is under consideration, the Minkowski form agrees with experimental results [87, 90, 92]. This maybe true in axion modified electrodynamics, as we can identify a similar guilty term due to eqn. (14) and hence (17). The non zero curl, should do active work without adding dissipation and should not be ignored in calculations of axion detector sensitivity. This extra term has all the properties of a “curl Force” [81, 82, 93], which adds spatial terms to the Poynting vector equations. In the following sections we compare the two ways of determining the power of photonic conversion for various axion haloscope topologies.

V. Resonant Cavity Haloscope

In this section we derive the sensitivity of an ADMX style radio frequency haloscope based on a cavity resonator [14–22], with a schematic shown in Fig. 1. First we undertake the calculation using the Abraham Poynting vector, as this is the a priori Poynting vector assumed

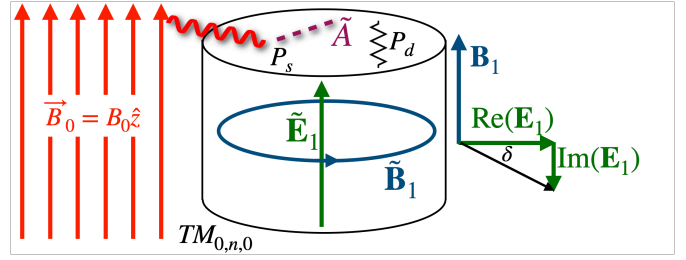


FIG. 1: Schematic of axion conversion in an ADMX style haloscope. Such haloscopes are based on radio frequency cavity resonators, where an external DC magnetic field, \vec{B}_0 , has a non-zero dot product with the non-dissipative electric field of the radio frequency mode in the cavity, $\text{Re}(\mathbf{E}_1)$. For a cylindrical cavity the sensitive modes are from the $TM_{0,n,0}$ mode family, where n is the radial mode number. The axial and azimuthal mode numbers must be zero. Finite losses means part of the electric field, $\text{Im}(\mathbf{E}_1)$, is in phase with the magnetic field, \mathbf{B}_1 , characterized by the loss angle δ , which for a high-Q system is very small and related by $\tan \delta \sim \frac{1}{Q_1}$.

across most of the literature, and then compare and contrast calculations using the Minkowski Poynting vector.

For a power source, P_s delivering energy to a resonator as shown in Fig. 1, the resonance is defined when the reactive power delivered by the source is zero, and thus when tuned on resonance the circulating energy only oscillates between the electric and magnetic energy in the resonator at the cavity resonance frequency, with no energy oscillating between the cavity and the power source (which in this case is the axion mixing with a DC magnetic field). In this case the power delivered to the cavity is real. This corresponds to the real part of the Poynting theorem equations, which we use in the next section to calculate the sensitivity of the axion haloscope. Internal to the cavity resonator, this circulating energy is described by a reactive (or imaginary) Poynting vector, which causes the power in the resonator to build up, with respect to the source input power, P_s . This build up is limited by the dissipation in the resonator and hence Q -factor. The build up of circulating power is given by $P_c = Q_1 P_s$, where in the steady state $P_s = P_d$, which is also related to the stored energy in the resonator, U_1 , by, $P_s = \omega_1 U_1$.

Thus, in such a cavity resonator the electric and magnetic field are out of phase (as opposed to a propagating wave, which are in phase) and in this paper we represent the lossless electric field vector phasor as real, and the lossless magnetic field vector phasor as imaginary (and so the cross product is imaginary). Dissipative terms, whether calculated in the volume or on the surface assume Ohms law, dictating that the dissipative part of the electric field be in phase with surface or volume currents and hence the magnetic field. Thus, the electric field effectively gains an imaginary component when losses are included. However, the majority of the electric field is real, with $\text{Im}(\vec{E}_1) \sim -\text{Re}(\vec{E}_1)/Q_1$. The tangential real part of the electric field must be continuous at the cavity

wall boundary, which for a perfect conductor is zero and sets the boundary conditions to calculate the frequency of the electromagnetic modes. Setting the reactive power to zero on resonance, allows us to calculate if there is any frequency shift of the bare cavity when excited by axions. We do find a small second order in Q-factor effect, calculated using Foster's reactance theorem [116]. However, there is no major impact on the sensitivity calculation, for completeness this is detailed in Appendix B and predicts a different value of frequency shift depending if we use the Minkowski or Abraham Poynting theorem.

A. Cavity Dissipated Power

Both Poynting vectors have a dissipative term in the real components, listed as the final term on the right hand side of eqns. (27) and (31) and graphically shown in Fig. 1. For dissipation effects over the volume, the volume current is in phase with the the imaginary part of the electric field, and is of the form, $\mathbf{J}_{e_1} = \sigma_e \mathbf{E}_1$, where σ_e is the effective conductivity of the volume, which is related to the loss tangent of the volume by $\sigma_e = \omega_a \epsilon_0 \tan \delta$ and given $\frac{1}{Q_1} \sim \tan \delta$, then $\mathbf{J}_{e_1} \sim \frac{\omega_a \epsilon_0}{Q_1} \mathbf{E}_1$, substituting these values in the last term on the right hand side of eqns. (27) or (31), the dissipated power in the cavity is calculated to be,

$$P_d = \frac{\omega_a \epsilon_0}{2Q_1} \int \mathbf{E}_1 \cdot \mathbf{E}_1^* dV = \frac{\omega_a U_1}{Q_1}. \quad (33)$$

For surface loss, the same volume integrals given by (27) and (31) collapse to surface integrals, where the surface current on the cavity walls is represented by the vector phasor, $\mathbf{K}_1 = \hat{n} \times \mathbf{H}_1$, of dimensions Amps/metre and the electric field at the surface is non-zero and in phase with the surface current, related by, $\mathbf{E}_1 = R_S \mathbf{K}_1$, where R_S is the surface resistance. Again, substituting these values in the last term on the right hand side of eqns. (27) or (31), means the dissipated power in the cavity is,

$$P_d = \frac{R_S}{2} \oint \mathbf{K}_1 \cdot \mathbf{K}_1^* ds = \frac{R_S}{2} \oint \mathbf{H}_1 \cdot \mathbf{H}_1^* ds = \frac{\omega_a U_1}{Q_1}, \quad (34)$$

which gives the same relationship with respect to the stored energy, U_1 and the dissipated power, whether it dissipates over the volume or over the surface of the cavity resonator.

B. Sensitivity from the Abraham Poynting Vector

In this calculation we assume the cavity is a closed system so there is no real power radiating outside the cavity volume, this means the closed surface integral on the left hand side of (31) should be set to zero ($\oint \text{Re}(\mathbf{S}_{EH}) \cdot \hat{n} ds = 0$). In practice power is taken outside the cavity due to the coupling, which in effect loads the cavity Q-factor, this phenomena may be added after the calculation using standard techniques. We also assume that the axion and the resonator frequency coincide ($\omega_1 = \omega_a$) and therefore the magnetic and electric energy inside the resonator will

be equal, again the effects of detuning may be added using standard techniques. Under these assumptions eqns. (31) becomes,

$$P_s = \frac{j g_{a\gamma\gamma} \omega_a c}{4} \int \vec{B}_0 \cdot (\tilde{a}^* \epsilon_0 \mathbf{E}_1 - \tilde{a} \epsilon_0 \mathbf{E}_1^*) dV = P_d = \frac{\omega_a U_1}{Q_1} \quad (35)$$

Here, P_s is the axion source power and must be real, note the source power is equal to the dissipated power, and as calculated in the last section can occur over the volume and/or over the cavity surface.

For the source power to be non-zero either, \mathbf{E}_1 or the axion scalar field, \tilde{a} , has to be imaginary. Since the axion scalar field is assumed to be lossless, we consider only the former to be imaginary, as has been suggested previously [106]. The general complex electric field is of the form, $\mathbf{E}_1 \approx (1 - j \tan \delta) \text{Re}(\mathbf{E}_1)$ in the regime where the loss angle is very small, $\delta \ll 1$. Hence, the axion source term in the steady state becomes,

$$P_s = \frac{g_{a\gamma\gamma} a_0 \omega_a \epsilon_0 c}{2Q_1} \int \vec{B}_0 \cdot \text{Re}(\mathbf{E}_1(\vec{r})) dV, \quad (36)$$

where $a_0 = \frac{1}{2}(\tilde{a} + \tilde{a}^*)$ is the peak value of the scalar axion field, so $a_0 = \sqrt{2}\langle a_0 \rangle$. Equating (36) to $P_d = \frac{\omega_a U_1}{Q_1}$ derived in (33) or (34) gives,

$$U_1 = \frac{g_{a\gamma\gamma} a_0 \epsilon_0 c}{2} \int \vec{B}_0 \cdot \text{Re}(\mathbf{E}_1) dV = \frac{\epsilon_0}{2} \int \mathbf{E}_1 \cdot \mathbf{E}_1^* dV, \quad (37)$$

Now defining the form factor of the cavity haloscope as

$$C_1 = \frac{\left(\int \vec{B}_0 \cdot \text{Re}(\mathbf{E}_1) dV \right)^2}{B_0^2 V_1 \int \mathbf{E}_1 \cdot \mathbf{E}_1^* dV}, \quad (38)$$

the axion induced circulating power may be calculated to be,

$$P_1 = \omega_a Q U_1 = g_{a\gamma\gamma}^2 \langle a_0 \rangle^2 \omega_a Q_1 \epsilon_0 c^2 B_0^2 V_1 C_1 = g_{a\gamma\gamma}^2 \rho_a Q_1 \epsilon_0 c^5 B_0^2 V_1 C_1 \frac{1}{\omega_a}, \quad (39)$$

where $\langle a_0 \rangle^2 = \frac{\rho_a}{c} \frac{\hbar^2}{m_a^2}$ and ρ_a is the axion dark matter density. This calculation is consistent with what has been derived previously [15, 31, 36].

C. Sensitivity from the Minkowski Poynting Vector

As before, assuming the real power inside the cavity haloscope is a closed system ($\oint \text{Re}(\mathbf{S}_{DB}) \cdot \hat{n} ds = 0$), the cavity is embedded inside a magnet ($\vec{J}_{e_0} \cdot (\tilde{a} c \mathbf{B}_1^* + \tilde{a}^* c \mathbf{B}_1) = 0$) and that the axion and the resonator frequency coincide ($\omega_1 = \omega_a$). Then, in this case eqn. (27) becomes,

$$P_s = \int \frac{1}{4} g_{a\gamma\gamma} c \vec{B}_0 \cdot (\tilde{a} \mathbf{J}_{e_1}^* + \tilde{a}^* \mathbf{J}_{e_1}) dV = P_d = \frac{\omega_a U_1}{Q_1} \quad (40)$$

Here, P_s is the axion source power and must be real.

As undertaken in the Abraham technique, we assume a lossy volume current in phase with the electric field of

the form, $\mathbf{J}_{e_1} = \sigma_e \mathbf{E}_1$ where, $\sigma_e = \frac{\omega_a \epsilon_0}{Q_1}$. Substituting the same value of \mathbf{J}_{e_1} into (40) gives,

$$P_s = \frac{g_{a\gamma\gamma} a_0 \omega_a \epsilon_0 c}{2Q_1} \int \vec{B}_0 \cdot \text{Re}(\mathbf{E}_1(\vec{r})) dV, \quad (41)$$

the same as calculated for the Abraham technique in eqn. (36), which means both eqns. (38) and (39) are calculable using both the Minkowski and Abraham Poynting vectors, and are consistent with previous sensitivity calculations for a standard ADMX style haloscope.

VI. Low-Mass Broadband Axion Haloscopes under DC Magnetic Field

For a low-mass broadband detector in the quasi-static limit, a haloscope may be inductive or capacitive and must be driven by reactive power from the source, so in the first approximation any dissipation or radiation loss can be ignored, and is thus set to zero. As before, we consider the generated electric field to be real ($\mathbf{E}_1^* = \mathbf{E}_1$) and the out of phase magnetic field as imaginary, ($\mathbf{B}_1^* = -\mathbf{B}_1$). Also, conduction currents will be in the same phase as the magnetic field and hence imaginary ($\mathbf{J}_{e_1}^* = -\mathbf{J}_{e_1}$). In this case, it is clear that real part of the delivered complex Poynting vector given by (31) and (27) must be zero, and the sensitivity of the reactive low-mass broadband haloscope will be determined from the imaginary reactive power delivered by the axion interacting with the background DC magnetic field.

There has been some recent controversy in the calculation of sensitivity for low mass reactive experiments in the quasi static limit, where the majority of the publications suggest that the sensitivity to electric field is suppressed when the Compton wave length of the axion is larger than the experimental dimensions [40, 106, 117, 118]. These experiments assume that the only modification to Maxwell's equations is due to the axion current (3), which is equivalent to assuming no boundary or spatial effects and thus setting the total derivative to zero. On the other hand, it has been shown that making these approximations too early in the calculation can lead to valid solutions being lost [61, 104, 119] due to extra spatial or surface terms, which in this case is due to the fact that $\vec{P}_{a1} = -g_{a\gamma\gamma} a(t) \epsilon_0 c \vec{B}_0(\vec{r})$ has a non-zero curl. Based on this, more sensitive experiments have been proposed using inductive wire loop readouts [61], or capacitive parallel plate readouts [104, 120]. In the following, as an example, we compare the sensitivity of a parallel plate capacitor to low mass axions by implementing both Poynting vector theorems.

A. Capacitor under DC Magnetic Field

For a parallel plate capacitor as shown in Fig.2 the last terms on the right hand side of eqns. (32) and (28) must be zero, since the conduction current must be zero in the lossless capacitor volume, this also means the third last term on the right hand side of (28) must be zero. Furthermore, if we assume the capacitor is embedded inside a DC magnet, the second last term in (28) must also be

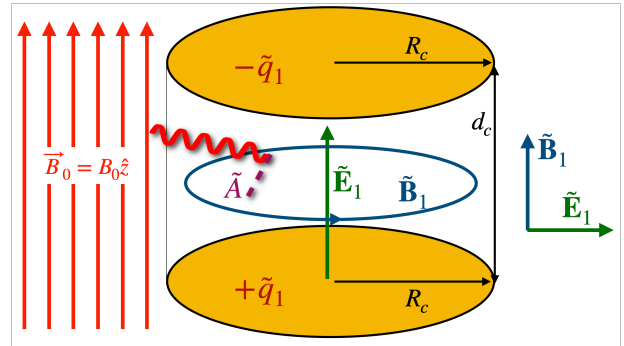


FIG. 2: Schematic of axion conversion in a Capacitive haloscope

zero (it is possible to make use of this term to make a sensitive low-mass detector [61]). This means the equations for reactive power flowing into and out of the capacitor volume, using the Abraham and Minkowski forms, are given by,

$$\oint j \text{Im}(\mathbf{S}_{EH}) \cdot \hat{n} ds = j\omega_a \int \left(\frac{1}{2\mu_0} \mathbf{B}_1^* \cdot \mathbf{B}_1 - \frac{\epsilon_0}{2} \mathbf{E}_1^* \cdot \mathbf{E}_1 + \frac{\epsilon_0}{2} g_{a\gamma\gamma} a_0 c \vec{B}_0 \cdot \text{Re}(\mathbf{E}_1) \right) dV, \quad (42)$$

and,

$$\oint j \text{Im}(\mathbf{S}_{DB}) \cdot \hat{n} ds = j\omega_a \int \left(\frac{1}{2\mu_0} \mathbf{B}_1^* \cdot \mathbf{B}_1 - \frac{\epsilon_0}{2} \mathbf{E}_1^* \cdot \mathbf{E}_1 + \epsilon_0 g_{a\gamma\gamma} a_0 c \vec{B}_0 \cdot \text{Re}(\mathbf{E}_1) \right) dV, \quad (43)$$

respectively.

For the capacitor in Fig.2 the AC electric field phasor, ignoring fringing is of the form;

$$\mathbf{E}_1 = \frac{\tilde{q}_1}{\pi R_c^2 \epsilon_0} \hat{z}, \quad (44)$$

where \tilde{q}_1 is the complex phasor of electric charge on the capacitor plates. Following this, from Ampere's law the AC magnetic field phasor within the capacitor volume ($V_c = \pi R_c^2 d_c$) may be calculated to be,

$$\mathbf{B}_1 = -j\omega_a \mu_0 \tilde{q}_1 \frac{r}{\pi R_c^2} \hat{\theta}, \quad (45)$$

Following this we may calculate the ratio of the magnetic energy density to electric energy density in the capacitor, given by,

$$\frac{\mathbf{B}_1 \cdot \mathbf{B}_1^*}{\epsilon_0 \mu_0 \mathbf{E}_1 \cdot \mathbf{E}_1^*} = \frac{r^2 \omega_a^2}{4c^2} = \frac{\pi^2 r^2}{\lambda_a^2}, \quad (46)$$

where λ_a is the Compton wavelength of the axion. Integrating over the volume of the capacitor, allows us to calculate the ratio of magnetic to electric energy to be (ignoring fringing),

$$\frac{\int_{V_c} \mathbf{B}_1 \cdot \mathbf{B}_1^* dV}{\epsilon_0 \mu_0 \int_{V_c} \mathbf{E}_1 \cdot \mathbf{E}_1^* dV} = \frac{R_c^2 \omega_a^2}{8c^2} = \frac{\pi^2 R_c^2}{2\lambda_a^2}. \quad (47)$$

These equations highlight that at DC the parallel plate capacitor is purely capacitive, but at AC the capacitor has a small but finite inductance in the quasi static limit, when $\lambda_a > R_c$. When $\lambda_a \sim R_c$, the capacitor could become resonant, similar to a $TM_{0,1,0}$ mode in a cylindrical cavity, however this would not be in the quasi-static limit. Nevertheless, in a circuit where the direction of the electric field, \mathbf{E}_1 in a capacitor is parallel to the applied DC magnetic field, \vec{B}_0 , eqn.(37) still holds for the capacitor, with an effective form factor of unity, which can be shown by substituting eqn. (44) into (38), and we can use this fact to help calculate the sensitivity of a low-mass capacitor experiment.

1. Sensitivity assuming the Abraham Poynting Vector

Assuming the Abraham Poynting vector, the reactive power delivered to and from a capacitor under DC magnetic field as shown in Fig.2 can be calculate by substituting eqn. (37) into (42) and using (46) we find,

$$jP_a = \oint j \operatorname{Im}(\mathbf{S}_{EH}) \cdot \hat{n} ds = \frac{j\omega_a g_{a\gamma\gamma} a_0 \epsilon_0 c}{2} \int (\vec{B}_0 \cdot \operatorname{Re}(\mathbf{E}_1)) \frac{\pi^2 r^2}{\lambda_a^2} dV, \quad (48)$$

Now, from the definition of the haloscope form factor (38), the reactive power delivered to the capacitor given by (48) becomes,

$$P_a = \omega_a U_c, \text{ where } U_c = g_{a\gamma\gamma}^2 \langle a_0 \rangle^2 \epsilon_0 c^2 B_0^2 V_1 \left(\frac{\pi^2 R_c^2}{2\lambda_a^2} \right)^2 \quad (49)$$

Thus the voltage phasor across the capacitor can be calculated from $U_c = \frac{1}{2} \tilde{\mathcal{V}} \tilde{\mathcal{V}}^* C_a$ ($C_a = \frac{\pi R_c^2 \epsilon_0}{d_c}$) to be,

$$\tilde{\mathcal{V}} = \sqrt{2} g_{a\gamma\gamma} \langle a_0 \rangle c B_0 d_c \left(\frac{\pi R_c}{\sqrt{2} \lambda_a} \right)^2 \quad (50)$$

which is consistent with an *rms* voltage across the capacitor of

$$\begin{aligned} \mathcal{V}_{rms} &= g_{a\gamma\gamma} \langle a_0 \rangle c B_0 d_c \left(\frac{\pi R_c}{\sqrt{2} \lambda_a} \right)^2 \\ &= g_{a\gamma\gamma} d_c \frac{c}{\omega_a} B_0 \sqrt{\rho_a c^3} \left(\frac{\pi R_c}{\sqrt{2} \lambda_a} \right)^2, \end{aligned} \quad (51)$$

where $\langle a_0 \rangle = \sqrt{\frac{\rho_a}{c} \frac{\hbar}{m_a}}$ and ρ_a is the axion dark matter density. This calculation is consistent with other calculations based on just the axion current [106, 117, 118], as given by eqn.(3), however does not take into account the non-zero value of the curl of \vec{P}_{a1} . The calculation predicts suppressed sensitivity at low-mass, proportional to $\frac{R_c^2}{\lambda_a^2}$.

2. Sensitivity assuming the Minkowski Poynting Vector

Assuming the Minkowski Poynting vector, the reactive power delivered to and from a capacitor under DC magnetic field as shown in Fig.2 can be calculate by substituting eqn. (37) into (43). Note in this case the magnetic energy is insignificant so ignoring this component, gives,

$$\begin{aligned} jP_a &= \oint j \operatorname{Im}(\mathbf{S}_{DB}) \cdot \hat{n} ds = \\ &\quad \frac{j\omega_a g_{a\gamma\gamma} a_0 \epsilon_0 c}{2} \int (\vec{B}_0 \cdot \operatorname{Re}(\mathbf{E}_1)) dV, \end{aligned} \quad (52)$$

Now, from the definition of the haloscope energy (37) and form factor (38), the energy stored in the capacitor (52) becomes,

$$U_c = g_{a\gamma\gamma}^2 \langle a_0 \rangle^2 \epsilon_0 c^2 B_0^2 V_1 \quad (53)$$

Thus the voltage phasor across the capacitor can be calculated from $U_c = \frac{1}{2} \tilde{\mathcal{V}} \tilde{\mathcal{V}}^* C_a$ to be,

$$\mathcal{V} = \sqrt{2} g_{a\gamma\gamma} \langle a_0 \rangle c B_0 d_c, \quad (54)$$

which is consistent with an *rms* voltage of

$$\mathcal{V}_{rms} = g_{a\gamma\gamma} \langle a_0 \rangle c B_0 d_c = g_{a\gamma\gamma} d_c \frac{c}{\omega_a} B_0 \sqrt{\rho_a c^3}, \quad (55)$$

which is the same as calculated previously [120]. Thus, we may conclude, from the Minkowski Poynting theorem, a sensitive low-mass experiment may be undertaken using a capacitive haloscope.

VII. Discussion and Conclusions

By applying Poynting theorem to axion modified electrodynamics, we have shown how the sensitivity of a resonant cavity and reactive broadband axion haloscope may be calculated. However, the way we apply the theorem is dependent on the type of detector. For example, Poynting vector analysis had already been undertaken to calculate the sensitivity of the MADMAX detector [42–45]. However, MADMAX is in the regime where the Compton wavelength of the axion is much smaller than the detector size, and is thus in a different regime to the resonant and reactive haloscope discussed in this paper. The MADMAX detector converts energy at a dielectric boundary, and is assumed to be in the propagating wave (or far field) limit, where the \vec{E} and \vec{B} vector phasors are in phase, so the Poynting vector is real and represents the physical energy flux leaving a surface, and propagates through the haloscope [42–44], and in principle can be made broadband.

In contrast, the resonant haloscope is generally the size of the Compton wavelength of the axion (unless higher order modes are implemented) and has an imaginary Poynting vector propagating internally within the resonator. This is because the axion induced photon energy produced within the resonator is reflected at the resonator boundaries, so the energy is localised in the

form of a standing wave. Thus, the propagating Poynting vector within the cavity is imaginary, with the $\tilde{\mathbf{E}}$ and $\tilde{\mathbf{B}}$ fields out of phase. In this work we have assumed the electric field is real, and thus the magnetic field is imaginary. However, on resonance (when $\omega_a = \omega_1$), the axion conversion process within the resonant cavity haloscope does not need to supply any reactive power, only real power. In this case the real part of the Poynting vector equation has both a source term and a dissipative term within the cavity, which are equal in the steady state, allowing the incident source power to escape the volume as heat, through the resistive losses. Meanwhile, reactive power flow oscillates between the electric and magnetic field within the cavity. The higher the Q-factor the more the circulating power builds up within the cavity, meaning the percentage of dissipation per cycle is smaller, and hence the detector sensitivity is proportional to the Q-factor. The down side is that the technique is narrow band, which requires complicated tuning mechanisms to scan for the axion of unknown mass.

On the other hand, low-mass experiments are in the quasi-static regime, where the Compton wavelength is much greater than the dimensions of the detector. In this case the sensitivity is determined by the reactive power flow within the detector created from the axion-photon

conversion. For the higher frequency cavity ADMX style haloscopes the implementation of either the Minkowski or Abraham axion modified Poynting vector has no significant influence on the calculated sensitivity. In contrast, for low-mass reactive haloscopes there is a large difference in sensitivity calculated from the two Poynting theorems. The Minkowski Poynting theorem picks up the extra non-conservative terms in the equations, which can be classified as a “curl force”. For electrodynamics in matter, it seems that the Minkowski Poynting vector is the correct one to use, in the situation when the curl of the polarization is non-zero. This also should be true for axion modified electrodynamics under a DC background magnetic field, $\vec{B}_0(\vec{r})$, because from eqn.(14), when $\nabla a = 0$, $\nabla \times \vec{P}_{a1} = -g_{a\gamma\gamma}a(t)c\epsilon_0\nabla \times \vec{B}_0(\vec{r}) = -\frac{g_{a\gamma\gamma}a(t)}{c}\vec{J}_{e1}$, which adds a spatial “curl force” term to the axion modified electrodynamical equations, due to the impressed current in the coil of the DC magnet. In most prior calculations this term has been ignored.

This work was funded by the ARC Centre of Excellence for Engineered Quantum Systems, CE170100009, and Dark Matter Particle Physics, CE200100008. BM was also funded by the Forrest Research Foundation.

- [1] R. D. Peccei and Helen R. Quinn. Cp conservation in the presence of pseudoparticles. *Phys. Rev. Lett.*, 38:1440–1443, Jun 1977.
- [2] F. Wilczek. Problem of strong p and t invariance in the presence of instantons. *Phys. Rev. Lett.*, 40:279–282, Jan 1978.
- [3] Steven Weinberg. A new light boson? *Phys. Rev. Lett.*, 40:223–226, Jan 1978.
- [4] Joerg Jaeckel and Andreas Ringwald. The low-energy frontier of particle physics. *Annual Review of Nuclear and Particle Science*, 60(1):405–437, 2010.
- [5] Jihn E. Kim. Weak-interaction singlet and strong CP invariance. *Phys. Rev. Lett.*, 43:103–107, Jul 1979.
- [6] Jihn E. Kim and Gianpaolo Carosi. Axions and the strong cp problem. *Rev. Mod. Phys.*, 82:557–601, Mar 2010.
- [7] A. R. Zhitnitsky. On possible suppression of the axion hadron interactions. (in russian). *Sov. J. Nucl. Phys.*, 31:260, 1980.
- [8] Michael Dine, Willy Fischler, and Mark Srednicki. A simple solution to the strong {CP} problem with a harmless axion. *Physics Letters B*, 104(3):199 – 202, 1981.
- [9] M.A. Shifman, A.I. Vainshtein, and V.I. Zakharov. Can confinement ensure natural {CP} invariance of strong interactions? *Nuclear Physics B*, 166(3):493 – 506, 1980.
- [10] Michael Dine and Willy Fischler. The not-so-harmless axion. *Physics Letters B*, 120(1):137 – 141, 1983.
- [11] John Preskill, Mark B. Wise, and Frank Wilczek. Cosmology of the invisible axion. *Physics Letters B*, 120(1):127 – 132, 1983.
- [12] L.F. Abbott and P. Sikivie. A cosmological bound on the invisible axion. *Physics Letters B*, 120(1–3):133 – 136, 1983.
- [13] J. Ipser and P. Sikivie. Can galactic halos be made of axions? *Phys. Rev. Lett.*, 50:925–927, Mar 1983.
- [14] P. Sikivie. Experimental tests of the “invisible” axion. *Phys. Rev. Lett.*, 51:1415–1417, Oct 1983.
- [15] P. Sikivie. Experimental tests of the “invisible” axion. *Phys. Rev. Lett.*, 52(8):695, 1984.
- [16] C. Hagmann, P. Sikivie, N. Sullivan, D. B. Tanner, and S.-I. Cho. Cavity design for a cosmic axion detector. *Review of Scientific Instruments*, 61(3):1076–1085, 1990.
- [17] C. Hagmann, P. Sikivie, N. S. Sullivan, and D. B. Tanner. Results from a search for cosmic axions. *Physical Review D*, 42(4):1297–1300, August 1990.
- [18] R. Bradley, J. Clarke, D. Kinion, L. J. Rosenberg, K. van Bibber, S. Matsuki, M. Muck, and P. Sikivie. Microwave cavity searches for dark-matter axions. *Rev. Mod. Phys.*, 75:777–817, 2003.
- [19] S. J. Asztalos, G. Carosi, C. Hagmann, D. Kinion, K. van Bibber, M. Hotz, L. J. Rosenberg, G. Rybka, J. Hoskins, J. Hwang, P. Sikivie, D. B. Tanner, R. Bradley, and J. Clarke. Squid-based microwave cavity search for dark-matter axions. *Phys. Rev. Lett.*, 104:041301, Jan 2010.
- [20] J. Hoskins, J. Hwang, C. Martin, P. Sikivie, N. S. Sullivan, D. B. Tanner, M. Hotz, L. J. Rosenberg, G. Rybka, A. Wagner, S. J. Asztalos, G. Carosi, C. Hagmann, D. Kinion, K. van Bibber, R. Bradley, and J. Clarke. Search for nonvirialized axionic dark matter. *Phys. Rev. D*, 84:121302, Dec 2011.
- [21] T. Braine, R. Cervantes, N. Crisosto, N. Du, S. Kimes,

L. J. Rosenberg, G. Rybka, J. Yang, D. Bowring, A. S. Chou, R. Khatiwada, A. Sonnenschein, W. Wester, G. Carosi, N. Woollett, L. D. Duffy, R. Bradley, C. Boutan, M. Jones, B. H. LaRoque, N. S. Oblath, M. S. Taubman, J. Clarke, A. Dove, A. Eddins, S. R. O’Kelley, S. Nawaz, I. Siddiqi, N. Stevenson, A. Agrawal, A. V. Dixit, J. R. Gleason, S. Jois, P. Sikivie, J. A. Solomon, N. S. Sullivan, D. B. Tanner, E. Lentz, E. J. Daw, J. H. Buckley, P. M. Harrington, E. A. Henriksen, and K. W. Murch. Extended search for the invisible axion with the axion dark matter experiment. *Phys. Rev. Lett.*, 124:101303, Mar 2020.

[22] ADMX Collaboration, C. Bartram, T. Braine, R. Cervantes, N. Crisosto, N. Du, G. Leum, L. J Rosenberg, G. Rybka, J. Yang, D. Bowring, A. S. Chou, R. Khatiwada, A. Sonnenschein, W. Wester, G. Carosi, N. Woollett, L. D. Duffy, M. Goryachev, B. McAllister, M. E. Tobar, C. Boutan, M. Jones, B. H. Laroque, N. S. Oblath, M. S. Taubman, John Clarke, A. Dove, A. Eddins, S. R. O’Kelley, S. Nawaz, I. Siddiqi, N. Stevenson, A. Agrawal, A. V. Dixit, J. R. Gleason, S. Jois, P. Sikivie, J. A. Solomon, N. S. Sullivan, D. B. Tanner, E. Lentz, E. J. Daw, M. G. Perry, J. H. Buckley, P. M. Harrington, E. A. Henriksen, and K. W. Murch. Axion dark matter experiment: Run 1b analysis details.

[23] Peter Svrcek and Edward Witten. Axions in string theory. *Journal of High Energy Physics*, 2006(06):051–051, jun 2006.

[24] Asimina Arvanitaki, Savas Dimopoulos, Sergei Dubovsky, Nemanja Kaloper, and John March-Russell. String axiverse. *Phys. Rev. D*, 81:123530, Jun 2010.

[25] Tetsutaro Higaki, Kazunori Nakayama, and Fuminobu Takahashi. Cosmological constraints on axionic dark radiation from axion-photon conversion in the early universe. *Journal of Cosmology and Astroparticle Physics*, 2013(09):030–030, sep 2013.

[26] Daniel Baumann, Daniel Green, and Benjamin Walsch. New target for cosmic axion searches. *Phys. Rev. Lett.*, 117:171301, Oct 2016.

[27] Raymond T. Co, Lawrence J. Hall, and Keisuke Harigaya. Axion kinetic misalignment mechanism. *Phys. Rev. Lett.*, 124:251802, Jun 2020.

[28] Raymond T. Co and Keisuke Harigaya. Axiogenesis. *Phys. Rev. Lett.*, 124:111602, Mar 2020.

[29] Raymond T. Co, Lawrence J. Hall, and Keisuke Harigaya. Predictions for axion couplings from alp cogenesis. *Journal of High Energy Physics*, 2021(1):172, 2021.

[30] V. K. Oikonomou. Unifying inflation with early and late dark energy epochs in axion $f(r)$ gravity. *Phys. Rev. D*, 103:044036, Feb 2021.

[31] Pierre Sikivie. Invisible axion search methods. *Rev. Mod. Phys.*, 93:015004, Feb 2021.

[32] Anton V. Sokolov and Andreas Ringwald. Photophilic hadronic axion from heavy magnetic monopoles. *Journal of High Energy Physics*, 2021(6):123, 2021.

[33] Luca Di Luzio, Maurizio Giannotti, Enrico Nardi, and Luca Visinelli. The landscape of qcd axion models. *Physics Reports*, 870:1–117, 2020. The landscape of QCD axion models.

[34] Jeff A. Dror, Hitoshi Murayama, and Nicholas L. Rodd. Cosmic axion background. *Phys. Rev. D*, 103:115004, Jun 2021.

[35] Alexandre Payez, Carmelo Evoli, Tobias Fischer, Maurizio Giannotti, Alessandro Mirizzi, and Andreas Ringwald. Revisiting the SN1987a gamma-ray limit on ultralight axion-like particles. *Journal of Cosmology and Astroparticle Physics*, 2015(02):006–006, feb 2015.

[36] Ben T. McAllister, Stephen R. Parker, and Michael E. Tobar. Axion Dark Matter Coupling to Resonant Photons via Magnetic Field. *Phys. Rev. Lett.*, 116(16):161804, 2016. [Erratum: *Phys. Rev. Lett.* 117,no.15,159901(2016)].

[37] R. Gupta, M. Anerella, A. Ghosh, W. Sampson, J. Schmalzle, D. Konikowska, Y. K. Semertzidis, and Y. Shin. High-field solenoid development for axion dark matter search at capp/ibs. *IEEE Transactions on Applied Superconductivity*, 26(4):1–5, June 2016.

[38] Ben T. McAllister, Stephen R. Parker, and Michael E. Tobar. 3D Lumped LC Resonators as Low Mass Axion Haloscopes. *Phys. Rev.*, D94(4):042001, 2016.

[39] Ben T. McAllister, Stephen R. Parker, Eugene N. Ivanov, and Michael E. Tobar. Cross-correlation signal processing for axion and wisp dark matter searches. *IEEE Transactions on Ultrasonics, Ferroelectrics, and Frequency Control*, 66(1):236–243, 2019.

[40] Yonatan Kahn, Benjamin R. Safdi, and Jesse Thaler. Broadband and Resonant Approaches to Axion Dark Matter Detection. *Phys. Rev. Lett.*, 117(14):141801, 2016.

[41] Ben T. McAllister, Graeme Flower, Eugene N. Ivanov, Maxim Goryachev, Jeremy Bourhill, and Michael E. Tobar. The organ experiment: An axion haloscope above 15 ghz. *Phys. Dark Universe*, 18:67–72, 2017.

[42] Allen Caldwell, Gia Dvali, Béla Majorovits, Alexander Millar, Georg Raffelt, Javier Redondo, Olaf Reimann, Frank Simon, and Frank Steffen. Dielectric haloscopes: A new way to detect axion dark matter. *Phys. Rev. Lett.*, 118:091801, Mar 2017.

[43] Alexander J. Millar, Georg G. Raffelt, Javier Redondo, and Frank D. Steffen. Dielectric haloscopes to search for axion dark matter: theoretical foundations. *Journal of Cosmology and Astroparticle Physics*, 2017(01):061–061, jan 2017.

[44] Ara N. Ioannisan, Narine Kazarian, Alexander J. Millar, and Georg G. Raffelt. Axion-photon conversion caused by dielectric interfaces: quantum field calculation. *Journal of Cosmology and Astroparticle Physics*, 2017(09):005–005, sep 2017.

[45] B. Majorovits and. MADMAX: A new road to axion dark matter detection. *Journal of Physics: Conference Series*, 1342:012098, jan 2020.

[46] B. M. Brubaker, L. Zhong, S. K. Lamoreaux, K. W. Lehnert, and K. A. van Bibber. Haystac axion search analysis procedure. *Phys. Rev. D*, 96:123008, Dec 2017.

[47] Junu Jeong, SungWoo Youn, Saebyeok Ahn, Jihn E. Kim, and Yannis K. Semertzidis. Concept of multiple-cell cavity for axion dark matter search. *Physics Letters B*, 777:412 – 419, 2018.

[48] Igor G. Irastorza and Javier Redondo. New experimental approaches in the search for axion-like particles. *Progress in Particle and Nuclear Physics*, 102:89–159, 2018.

[49] Jonathan L. Ouellet, Chiara P. Salemi, Joshua W. Foster, Reyco Henning, Zachary Bogorad, Janet M. Conrad, Joseph A. Formaggio, Yonatan Kahn, Joe Mervini, Alexey Radovinsky, Nicholas L. Rodd, Benjamin R. Safdi, Jesse Thaler, Daniel Winklehner, and

Lindley Winslow. Design and implementation of the abracadabra-10 cm axion dark matter search. *Phys. Rev. D*, 99:052012, Mar 2019.

[50] Koji Nagano, Tomohiro Fujita, Yuta Michimura, and Ippei Obata. Axion dark matter search with interferometric gravitational wave detectors. *Physical Review Letters*, 123(11), sep 2019.

[51] Maxim Goryachev, Ben T. McAllister, and Michael E. Tobar. Axion detection with precision frequency metrology. *Physics of the Dark Universe*, 26:100345, dec 2019.

[52] J. Choi, H. Themann, M. J. Lee, B. R. Ko, and Y. K. Semertzidis. First axion dark matter search with toroidal geometry. *Phys. Rev. D*, 96:061102, Sep 2017.

[53] Reyco Henning et al. First results from abracadabra-10 cm: A search for sub- μ ev axion dark matter. *Phys. Rev. Lett.*, 122(1810.12257), 2019.

[54] Hongwan Liu, Brodi D. Elwood, Matthew Evans, and Jesse Thaler. Searching for axion dark matter with birefringent cavities. *Physical Review D*, 100(2), jul 2019.

[55] David J. E. Marsh, Kin Chung Fong, Erik W. Lentz, Libor Šmejkal, and Mazhar N. Ali. Proposal to detect dark matter using axionic topological antiferromagnets. *Phys. Rev. Lett.*, 123:121601, Sep 2019.

[56] Jan Schütte-Engel, David J.E. Marsh, Alexander J. Millar, Akihiko Sekine, Francesca Chadha-Day, Sebastian Hoof, Mazhar N. Ali, Kin Chung Fong, Edward Hardy, and Libor Šmejkal. Axion quasiparticles for axion dark matter detection. *Journal of Cosmology and Astroparticle Physics*, 2021(08):066, aug 2021.

[57] Matthew Lawson, Alexander J. Millar, Matteo Pandolfi, Edoardo Vitagliano, and Frank Wilczek. Tunable axion plasma haloscopes. *Phys. Rev. Lett.*, 123:141802, Oct 2019.

[58] V. Anastassopoulos, S. Aune, K. Barth, A. Belov, H. Bräuninger, G. Cantatore, J. M. Carmona, J. F. Castel, S. A. Cetin, F. Christensen, J. I. Collar, T. Dafni, M. Davenport, T. A. Decker, A. Dermenev, K. Desch, C. Eleftheriadis, G. Fanourakis, E. Ferrer-Ribas, H. Fischer, J. A. García, A. Gardikiotis, J. G. Garza, E. N. Gazis, T. Geralis, I. Giomataris, S. Glinenko, C. J. Hailey, M. D. Hasinoff, D. H. H. Hoffmann, F. J. Iguaz, I. G. Irastorza, A. Jakobsen, J. Jacoby, K. Jakovčić, J. Kaminski, M. Karuza, N. Kralj, M. Krčmar, S. Kostoglou, Ch. Krieger, B. Lakić, J. M. Laurent, A. Liolios, A. Ljubičić, G. Luzón, M. Maroudas, L. Miceli, S. Neff, I. Ortega, T. Papaevangelou, K. Paraschou, M. J. Pivovaroff, G. Raffelt, M. Rosu, J. Ruz, E. Ruiz Chóliz, I. Savvidis, S. Schmidt, Y. K. Semertzidis, S. K. Solanki, L. Stewart, T. Vafeiadis, J. K. Vogel, S. C. Yıldız, K. Zioutas, and CAST Collaboration. New cast limit on the axion-photon interaction. *Nature Physics*, 13(6):584–590, 2017.

[59] L. Zhong, S. Al Kenany, K. M. Backes, B. M. Brubaker, S. B. Cahn, G. Carosi, Y. V. Gurevich, W. F. Kindel, S. K. Lamoreaux, K. W. Lehnert, S. M. Lewis, M. Malnou, R. H. Maruyama, D. A. Palken, N. M. Rapidis, J. R. Root, M. Simanovskaia, T. M. Shokair, D. H. Speller, I. Urdinaran, and K. A. van Bibber. Results from phase 1 of the haystac microwave cavity axion experiment. *Phys. Rev. D*, 97:092001, May 2018.

[60] S. Lee, S. Ahn, J. Choi, B. R. Ko, and Y. K. Semertzidis. Axion dark matter search around 6.7 μ eV. *Phys. Rev. Lett.*, 124:101802, Mar 2020.

[61] Michael E. Tobar, Ben T. McAllister, and Maxim Goryachev. Broadband electrical action sensing techniques with conducting wires for low-mass dark matter axion detection. *Physics of the Dark Universe*, 30:100624, 2020.

[62] Graciela B. Gelmini, Alexander J. Millar, Volodymyr Takhistov, and Edoardo Vitagliano. Probing dark photons with plasma haloscopes. *Phys. Rev. D*, 102:043003, Aug 2020.

[63] Asher Berlin, Raffaele Tito D’Agnolo, Sebastian AR Ellis, Christopher Nantista, Jeffrey Neilson, Philip Schuster, Sami Tantawi, Natalia Toro, and Kevin Zhou. Axion dark matter detection by superconducting resonant frequency conversion. *Journal of High Energy Physics*, 2020(7):1–42, 2020.

[64] Robert Lasenby. Parametrics of electromagnetic searches for axion dark matter. *Phys. Rev. D*, 103:075007, Apr 2021.

[65] Alexander V. Gramolin, Deniz Aybas, Dorian Johnson, Janos Adam, and Alexander O. Sushkov. Search for axion-like dark matter with ferromagnets. *Nature Physics*, 17(1):79–84, 2021.

[66] A. Abeln, K. Altenmüller, S. Arguedas Cuendis, E. Armengaud, D. Attié, S. Aune, S. Basso, L. Bergé, B. Biazzu, P. T. C. Borges De Sousa, P. Brun, N. Bykovskiy, D. Calvet, J. M. Carmona, J. F. Castel, S. Cebrián, V. Chernov, F. E. Christensen, M. M. Civitani, C. Co-gollos, T. Dafní, A. Derbin, K. Desch, D. Díez, M. Dinter, B. Döbrich, I. Drachnev, A. Dudarev, L. Dumoulin, D. D. M. Ferreira, E. Ferrer-Ribas, I. Fleck, J. Galán, D. Gascón, L. Gastaldo, M. Giannotti, Y. Giomataris, A. Giuliani, S. Glinenko, J. Golm, N. Golubev, L. Hagge, J. Hahn, C. J. Hailey, D. Hengstler, P. L. Henriksen, T. Houdy, R. Iglesias-Marzoa, F. J. Iguaz, I. G. Irastorza, C. Iñiguez, K. Jakovčić, J. Kaminski, B. Kanoute, S. Karstensen, L. Kravchuk, B. Lakić, T. Lasserre, P. Laurent, O. Limousin, A. Lindner, M. Loidl, I. Lomskaya, G. López-Alegre, B. Lubsandorzhiev, K. Ludwig, G. Luzón, C. Malbrunot, C. Margalejo, A. Marin-Franch, S. Marnieros, F. Marutzky, J. Mauricio, Y. Menesguen, M. Mentink, S. Mertens, F. Mescia, J. Miralda-Escudé, H. Mirallas, J. P. Mols, V. Muratova, X. F. Navick, C. Nones, A. Notari, A. Nozik, L. Obis, C. Oriol, F. Orsini, A. Ortiz de Solórzano, S. Oster, H. P. Pais Da Silva, V. Pantuev, T. Papaevangelou, G. Pareschi, K. Perez, O. Pérez, E. Picatoste, M. J. Pivovaroff, D. V. Poda, J. Redondo, A. Ringwald, M. Rodrigues, F. Rueda-Teruel, S. Rueda-Teruel, E. Ruiz-Chóliz, J. Ruz, E. O. Saemann, J. Salvado, T. Schiffer, S. Schmidt, U. Schneekloth, M. Schott, L. Segui, F. Tavecchio, H. H. J. ten Kate, I. Tkachev, S. Troitsky, D. Unger, E. Unzhakov, N. Ushakov, J. K. Vogel, D. Voronin, A. Weltman, U. Werthenbach, W. Wuensch, A. Yanes-Díaz, and The IAXO collaboration. Conceptual design of baby-iaxo, the intermediate stage towards the international axion observatory. *Journal of High Energy Physics*, 2021(5):137, 2021.

[67] Catriona A. Thomson, Ben T. McAllister, Maxim Goryachev, Eugene N. Ivanov, and Michael E. Tobar. Upconversion loop oscillator axion detection experiment: A precision frequency interferometric axion dark matter search with a cylindrical microwave cavity. *Phys. Rev. Lett.*, 126:081803, 2021.

[68] Claudio Gatti, Paola Gianotti, Carlo Ligi, Mauro Raggi,

and Paolo Valente. Dark matter searches at *Inf. Universe*, 7(7), 2021.

[69] Y Kishimoto, Y Suzuki, I Ogawa, Y Mori, and M Yamashita. Development of a cavity with photonic crystal structure for axion searches. *Progress of Theoretical and Experimental Physics*, 2021(6), 04 2021. 063H01.

[70] Jack A. Devlin, Matthias J. Borchert, Stefan Erlewein, Markus Fleck, James A. Harrington, Barbara Latacz, Jan Warncke, Elise Wursten, Matthew A. Bohman, Andreas H. Mooser, Christian Smorra, Markus Wiesinger, Christian Will, Klaus Blaum, Yasuyuki Matsuda, Christian Ospelkaus, Wolfgang Quint, Jochen Walz, Yasunori Yamazaki, and Stefan Ulmer. Constraints on the coupling between axionlike dark matter and photons using an antiproton superconducting tuned detection circuit in a cryogenic penning trap. *Phys. Rev. Lett.*, 126:041301, Jan 2021.

[71] Ohjoon Kwon, Doyu Lee, Woohyun Chung, Danho Ahn, HeeSu Byun, Fritz Caspers, Hyoungsoon Choi, Jihoon Choi, Yonuk Chung, Hoyong Jeong, Junu Jeong, Jihn E. Kim, Jinsu Kim, Ça ğlar Kutlu, Jihnhwan Lee, Myeong-Jae Lee, Soohyung Lee, Andrei Matlashov, Seonjeong Oh, Seongtae Park, Sergey Uchaikin, SungWoo Youn, and Yannis K. Semertzidis. First results from an axion haloscope at capp around 10.7 μ eV. *Phys. Rev. Lett.*, 126:191802, May 2021.

[72] K. M. Backes, D. A. Palken, S. Al Kenany, B. M. Brubaker, S. B. Cahn, A. Droster, Gene C. Hilton, Sumita Ghosh, H. Jackson, S. K. Lamoreaux, A. F. Leder, K. W. Lehnert, S. M. Lewis, M. Malnou, R. H. Maruyama, N. M. Rapidis, M. Simanovskia, Sukhman Singh, D. H. Speller, I. Urdinaran, Leila R. Vale, E. C. van Assendelft, K. van Bibber, and H. Wang. A quantum enhanced search for dark matter axions. *Nature*, 590(7845):238–242, 2021.

[73] Aichi Iwazaki. Axion-radiation conversion by super and normal conductors. *Nuclear Physics B*, 963:115298, 2021.

[74] So Chigusa, Takeo Moroi, and Kazunori Nakayama. Axion/hidden-photon dark matter conversion into condensed matter axion. *Journal of High Energy Physics*, 2021(8):74, 2021.

[75] Xunyu Liang, Egor Peshkov, Ludovic Van Waerbeke, and Ariel Zhitnitsky. Proposed network to detect axion quark nugget dark matter. *Phys. Rev. D*, 103:096001, May 2021.

[76] D. J. White and P. L. Overfelt. Poynting's theorems and their relationship to antenna power, q , and bandwidth. *Office of Naval Research NAWCWPNS Technical Publication*, (8419), 1999.

[77] Keqian Zhang and Dejie Li. *Electromagnetic Theory for Microwaves and Optoelectronics*. Springer, 2nd edition, 2008.

[78] John L. Volakis and Kubilay Sertel. *Integral Equation Methods for Electromagnetics*. Scitech Publishing Inc., 911 Paverstone Drive, Suite B, Raleigh, NC 27615, 2012.

[79] Constantine A Balanis. *Advanced Engineering Electromagnetics*. John Wiley, 2012.

[80] Roger E. Harrington. *Introduction to Electromagnetic Engineering*. Dover Publications, Inc., 31 East 2nd Street, Mineola, NY 11501, 2nd edition, 2012.

[81] Pinyu Wu, Rongxin Huang, Christian Tischer, Alexander Jonas, and Ernst-Ludwig Florin. Direct measurement of the nonconservative force field generated by optical tweezers. *Phys. Rev. Lett.*, 103:108101, Sep 2009.

[82] M V Berry and Pragya Shukla. Physical curl forces: dipole dynamics near optical vortices. *Journal of Physics A: Mathematical and Theoretical*, 46(42):422001, oct 2013.

[83] Max Bethune-Waddell and Kenneth J Chau. Simulations of radiation pressure experiments narrow down the energy and momentum of light in matter. *Reports on Progress in Physics*, 78(12):122401, oct 2015.

[84] Sergey Sukhov and Aristide Dogariu. Non-conservative optical forces. *Reports on Progress in Physics*, 80(11):112001, sep 2017.

[85] Partha Guha. Curl forces and their role in optics and ion trapping. *The European Physical Journal D*, 74(5):99, 2020.

[86] D. F. Nelson. Momentum, pseudomomentum, and wave momentum: Toward resolving the minkowski-abraham controversy. *Phys. Rev. A*, 44:3985–3996, Sep 1991.

[87] David J. Griffiths. Resource letter em-1: Electromagnetic momentum. *American Journal of Physics*, 80(1):7–18, 2012.

[88] Masud Mansuripur. Force, torque, linear momentum, and angular momentum in classical electrodynamics. *Applied Physics A*, 123(10):653, 2017.

[89] V.P. Torchigin. Dozen arguments in favor of the minkowski form of the momentum of light in matter. *Optik*, 218:164986, 2020.

[90] R. N. C. Pfeifer, T. A. Nieminen, N. R. Heckenberg, and H. Rubinsztein-Dunlop. Colloquium: Momentum of an electromagnetic wave in dielectric media. *Rev. Mod. Phys.*, 79:1197–1216, Oct 2007.

[91] Ulf Leonhardt. Momentum in an uncertain light. *Nature*, 444(7121):823–824, 2006.

[92] Stephen M. Barnett. Resolution of the abraham-minkowski dilemma. *Phys. Rev. Lett.*, 104:070401, Feb 2010.

[93] Berry M. V. and Shukla Pragya. Hamiltonian curl forces. *Proc. R. Soc. A.*, 471:20150002, 2015.

[94] P Strange. Quantized hamiltonian curl forces and squeezed light. *Journal of Physics A: Mathematical and Theoretical*, 51(33):335303, jul 2018.

[95] M V Berry. Classical and quantum complex hamiltonian curl forces. *Journal of Physics A: Mathematical and Theoretical*, 53(41):415201, sep 2020.

[96] Aurélien Drezet. Dual-lagrangian description adapted to quantum optics in dispersive and dissipative dielectric media. *Phys. Rev. A*, 94:053826, Nov 2016.

[97] Paul Kinsler, Alberto Favaro, and Martin W McCall. Four poynting theorems. *European Journal of Physics*, 30(5):983–993, jul 2009.

[98] Hermann Minkowski. Die grundgleichungen für die elektromagnetischen vorgänge in bewegten körpern. *Nachrichten von der Gesellschaft der Wissenschaften zu Göttingen, Mathematisch-Physikalische Klasse*, pages 53–111, 1908.

[99] J. C. Garrison and R. Y. Chiao. Canonical and kinetic forms of the electromagnetic momentum in an ad hoc quantization scheme for a dispersive dielectric. *Phys. Rev. A*, 70:053826, Nov 2004.

[100] Max Abraham. Zur elektrodynamik bewegter körper. *Rendiconti del Circolo Matematico di Palermo (1884-1940)*, 28(1):1, 2009.

[101] Max Abraham. Sullelettrodinamica di minkowski. *Rendiconti del Circolo Matematico di Palermo (1884-1940)*,

30(1):33–46, 1910.

[102] Michael E. Tobar, Ben T. McAllister, and Maxim Goryachev. Electrodynamics of free- and bound-charge electricity generators using impressed sources. *Phys. Rev. Applied*, 15:014007, Jan 2021.

[103] Michael E. Tobar, Raymond Y. Chiao, and Maxim Goryachev. Active dipoles, electric vector potential and berry phase. *arXiv:2101.00945 [physics.class-ph]*, 2021.

[104] Michael E. Tobar, Ben T. McAllister, and Maxim Goryachev. Modified axion electrodynamics as impressed electromagnetic sources through oscillating background polarization and magnetization. *Physics of the Dark Universe*, 26:100339, 2019.

[105] Frank Wilczek. Two applications of axion electrodynamics. *Physical Review Letters*, 58(18):1799–1802, 05 1987.

[106] Younggeun Kim, Dongok Kim, Junu Jeong, Jinsu Kim, Yun Chang Shin, and Yannis K. Semertzidis. Effective approximation of electromagnetism for axion haloscope searches. *Physics of the Dark Universe*, 26:100362, 2019.

[107] Luca Visinelli. Axion-electromagnetic waves. *Modern Physics Letters A*, 28(35):1350162, 2013.

[108] Andreas Asker. *Axion Electrodynamics and Measurable Effects in Topological Insulators*. Kaaerstads University, 2018.

[109] Robert P Cameron and Stephen M Barnett. Electromagnetic symmetry and noether’s theorem. *New Journal of Physics*, 14(12):123019, dec 2012.

[110] Robert P Cameron, Stephen M Barnett, and Alison M Yao. Optical helicity, optical spin and related quantities in electromagnetic theory. *New Journal of Physics*, 14(5):053050, may 2012.

[111] Konstantin Y Bliokh, Aleksandr Y Bekshaev, and Franco Nori. Dual electromagnetism: helicity, spin, momentum and angular momentum. *New Journal of Physics*, 15(3):033026, mar 2013.

[112] Konstantin Y Bliokh, Aleksandr Y Bekshaev, and Franco Nori. Corrigendum: Dual electromagnetism: helicity, spin, momentum, and angular momentum (2013new j. phys.15033026). *New Journal of Physics*, 18(8):089503, aug 2016.

[113] S. A. Schelkunoff. Some equivalence theorems of electromagnetics and their application to radiation problems. *The Bell System Technical Journal*, 15(1):92–112, 1936.

[114] C. G. Montgomery, R. H. Dicke, and E. M. Purcell. (eds) *Principles of Microwave Circuits*. McGraw-Hill, 1987.

[115] R. H. Dicke. *General Microwave Circuit Theorems*, chapter 5, pages 130–161. Principles of Microwave Circuits, McGraw-Hill, 1987.

[116] Ronald M. Foster. A reactance theorem. *The Bell System Technical Journal*, 3(2):259–267, 1924.

[117] Jonathan Ouellet and Zachary Bogorad. Solutions to axion electrodynamics in various geometries. *Phys. Rev. D*, 99:055010, Mar 2019.

[118] Marc Beutter, Andreas Pargner, Thomas Schwetz, and Elisa Todarello. Axion-electrodynamics: a quantum field calculation. *Journal of Cosmology and Astroparticle Physics*, 2019(02):026–026, feb 2019.

[119] ChunJun Cao and Ariel Zhitnitsky. Axion detection via topological casimir effect. *Phys. Rev. D*, 96:015013, Jul 2017.

[120] Ben T. McAllister, Maxim Goryachev, Jeremy Bourhill, Eugene N. Ivanov, and Michael E. Tobar. Broadband axion dark matter haloscopes via electric field sensing. *arXiv:1803.07755 [physics.ins-det]*, 2018.

[121] Robert Beringer. *Resonant cavities as microwave circuit elements*, chapter 7, pages 207–239. Principles of Microwave Circuits, McGraw-Hill, 1987.

VIII. Appendix A: Derivation of Poynting Theorem Equations

In this appendix we derive equations (27), (28), (31) and (32) in the main text.

A. Axion Modified Minkowski Poynting Theorem

To derive eqn. (27) and (28), we begin with writing the divergence of the real and imaginary part of \mathbf{S}_{DB} as,

$$\begin{aligned}\nabla \cdot \text{Re}(\mathbf{S}_{DB}) &= \frac{1}{2} \nabla \cdot (\mathbf{S}_{DB} + \mathbf{S}_{DB}^*) \\ \nabla \cdot \text{Im}(\mathbf{S}_{DB}) &= \frac{1}{2} \nabla \cdot (\mathbf{S}_{DB} - \mathbf{S}_{DB}^*)\end{aligned}\quad (56)$$

The next step is to calculate $\nabla \cdot \mathbf{S}_{DB}$ and $\nabla \cdot \mathbf{S}_{DB}^*$,

$$\begin{aligned}\nabla \cdot \mathbf{S}_{DB} &= \frac{1}{2} \nabla \cdot \left(\frac{1}{\epsilon_0} \mathbf{D}_1 \times \frac{1}{\mu_0} \mathbf{B}_1^* \right) = \\ &\frac{1}{2} \left(\frac{1}{\mu_0} \mathbf{B}_1^* \cdot \frac{1}{\epsilon_0} \nabla \times \mathbf{D}_1 - \frac{1}{\epsilon_0} \mathbf{D}_1 \cdot \frac{1}{\mu_0} \nabla \times \mathbf{B}_1^* \right),\end{aligned}\quad (57)$$

and,

$$\begin{aligned}\nabla \cdot \mathbf{S}_{DB}^* &= \frac{1}{2} \nabla \cdot \left(\frac{1}{\epsilon_0} \mathbf{D}_1^* \times \frac{1}{\mu_0} \mathbf{B}_1 \right) = \\ &\frac{1}{2} \left(\frac{1}{\mu_0} \mathbf{B}_1 \cdot \frac{1}{\epsilon_0} \nabla \times \mathbf{D}_1^* - \frac{1}{\epsilon_0} \mathbf{D}_1^* \cdot \frac{1}{\mu_0} \nabla \times \mathbf{B}_1 \right).\end{aligned}\quad (58)$$

In harmonic form, the axion modified Ampere’s and Faraday’s law under a background DC B-field of $\vec{B}_0(\vec{r})$, created by an impressed electrical DC current in the magnet coil, \vec{J}_{e_0} , may be written as,

$$\begin{aligned}\frac{1}{\mu_0} \nabla \times \mathbf{B}_1 &= \mathbf{J}_{e_1} - j\omega_1 \epsilon_0 \mathbf{E}_1 + j\omega_a g_{a\gamma\gamma} \epsilon_0 c \vec{B}_0 \tilde{a} \\ \frac{1}{\mu_0} \nabla \times \mathbf{B}_1^* &= \mathbf{J}_{e_1}^* + j\omega_1 \epsilon_0 \mathbf{E}_1^* - j\omega_a g_{a\gamma\gamma} \epsilon_0 c \vec{B}_0 \tilde{a}^* \\ \frac{1}{\epsilon_0} \nabla \times \mathbf{D}_1 &= j\omega_1 \mathbf{B}_1 - g_{a\gamma\gamma} c \mu_0 \tilde{a} \vec{J}_{e_0} \\ \frac{1}{\epsilon_0} \nabla \times \mathbf{D}_1^* &= -j\omega_1 \mathbf{B}_1^* - g_{a\gamma\gamma} c \mu_0 \tilde{a}^* \vec{J}_{e_0}.\end{aligned}\quad (59)$$

Substituting eqns. (59) into eqns. (57) and (58) leads to.

$$\begin{aligned}\nabla \cdot \mathbf{S}_{DB} &= \frac{1}{2\mu_0} \mathbf{B}_1^* \cdot (j\omega_1 \mathbf{B}_1 - g_{a\gamma\gamma} \tilde{a} c \mu_0 \vec{J}_{e_0}) - \\ &\frac{1}{2} (\mathbf{E}_1 - g_{a\gamma\gamma} \tilde{a} c \vec{B}_0) \cdot (\mathbf{J}_{e_1}^* + j\omega_1 \epsilon_0 \mathbf{E}_1^* - j\omega_a g_{a\gamma\gamma} \epsilon_0 \tilde{a}^* c \vec{B}_0) \\ &= \frac{j\omega_1}{2} \left(\frac{1}{\mu_0} \mathbf{B}_1^* \cdot \mathbf{B}_1 - \epsilon_0 \mathbf{E}_1 \cdot \mathbf{E}_1^* \right) + \frac{j\omega_1}{2} \epsilon_0 g_{a\gamma\gamma} \tilde{a} c \vec{B}_0 \cdot \mathbf{E}_1^* \\ &+ \frac{j\omega_a}{2} g_{a\gamma\gamma} \epsilon_0 \tilde{a}^* c \vec{B}_0 \cdot \mathbf{E}_1 - \frac{1}{2} \mathbf{E}_1 \cdot \mathbf{J}_{e_1}^* + \frac{1}{2} g_{a\gamma\gamma} \tilde{a} c \vec{B}_0 \cdot \mathbf{J}_{e_1}^* \\ &- \frac{1}{2} g_{a\gamma\gamma} \tilde{a} c \mathbf{B}_1^* \cdot \vec{J}_{e_0},\end{aligned}\quad (60)$$

and,

$$\begin{aligned}
\nabla \cdot \mathbf{S}_{DB}^* &= \frac{1}{2\mu_0} \mathbf{B}_1 \cdot (-j\omega_1 \mathbf{B}_1^* - g_{a\gamma\gamma} \tilde{a}^* c \mu_0 \vec{J}_{e_0}) - \\
&\frac{1}{2} (\mathbf{E}_1^* - g_{a\gamma\gamma} \tilde{a}^* c \vec{B}_0) \cdot (\mathbf{J}_{e_1} - j\omega_1 \epsilon_0 \mathbf{E}_1 + j\omega_a g_{a\gamma\gamma} \epsilon_0 \tilde{a} c \vec{B}_0) \\
&= \frac{j\omega_1}{2} \left(\epsilon_0 \mathbf{E}_1 \cdot \mathbf{E}_1^* - \frac{1}{\mu_0} \mathbf{B}_1^* \cdot \mathbf{B}_1 \right) - \frac{j\omega_1}{2} \epsilon_0 g_{a\gamma\gamma} \tilde{a}^* c \vec{B}_0 \cdot \mathbf{E}_1 \\
&- \frac{j\omega_a}{2} g_{a\gamma\gamma} \epsilon_0 \tilde{a} c \vec{B}_0 \cdot \mathbf{E}_1^* - \frac{1}{2} \mathbf{E}_1^* \cdot \mathbf{J}_{e_1} + \frac{1}{2} g_{a\gamma\gamma} \tilde{a}^* c \vec{B}_0 \cdot \mathbf{J}_{e_1} \\
&- \frac{1}{2} g_{a\gamma\gamma} \tilde{a}^* c \mathbf{B}_1 \cdot \vec{J}_{e_0}
\end{aligned} \tag{61}$$

Now by substituting (60) and (60) into (56) we obtain,

$$\begin{aligned}
\nabla \cdot \text{Re}(\mathbf{S}_{DB}) &= \frac{j(\omega_1 - \omega_a)}{4} \epsilon_0 g_{a\gamma\gamma} c \vec{B}_0 \cdot (\tilde{a} \mathbf{E}_1^* - \tilde{a}^* \mathbf{E}_1) \\
&+ \frac{1}{4} g_{a\gamma\gamma} c \vec{B}_0 \cdot (\tilde{a} \mathbf{J}_{e_1}^* + \tilde{a}^* \mathbf{J}_{e_1}) - \frac{1}{4} g_{a\gamma\gamma} \vec{J}_{e_0} \cdot (\tilde{a}^* c \mathbf{B}_1 + \tilde{a} c \mathbf{B}_1^*) \\
&- \frac{1}{4} (\mathbf{E}_1 \cdot \mathbf{J}_{e_1}^* + \mathbf{E}_1^* \cdot \mathbf{J}_{e_1}),
\end{aligned} \tag{62}$$

and

$$\begin{aligned}
\nabla \cdot j \text{Im}(\mathbf{S}_{DB}) &= \frac{j\omega_1}{2} \left(\frac{1}{\mu_0} \mathbf{B}_1^* \cdot \mathbf{B}_1 - \epsilon_0 \mathbf{E}_1 \cdot \mathbf{E}_1^* \right) \\
&+ \frac{j(\omega_1 + \omega_a)}{4} \epsilon_0 g_{a\gamma\gamma} c \vec{B}_0 \cdot (\tilde{a} \mathbf{E}_1^* + \tilde{a}^* \mathbf{E}_1) + \\
&\frac{1}{4} g_{a\gamma\gamma} c \vec{B}_0 \cdot (\tilde{a} \mathbf{J}_{e_1}^* - \tilde{a}^* \mathbf{J}_{e_1}) + \frac{1}{4} g_{a\gamma\gamma} \vec{J}_{e_0} \cdot (\tilde{a}^* c \mathbf{B}_1 - \tilde{a} c \mathbf{B}_1^*) \\
&- \frac{1}{4} (\mathbf{E}_1 \cdot \mathbf{J}_{e_1}^* - \mathbf{E}_1^* \cdot \mathbf{J}_{e_1})
\end{aligned} \tag{63}$$

Then applying the divergence theorem, we arrive at,

$$\begin{aligned}
\oint \text{Re}(\mathbf{S}_{DB}) \cdot \hat{n} ds &= \\
\int \left(\frac{j(\omega_1 - \omega_a)}{4} \epsilon_0 g_{a\gamma\gamma} c \vec{B}_0 \cdot (\tilde{a} \mathbf{E}_1^* - \tilde{a}^* \mathbf{E}_1) \right. & \\
&+ \frac{1}{4} g_{a\gamma\gamma} c \vec{B}_0 \cdot (\tilde{a} \mathbf{J}_{e_1}^* + \tilde{a}^* \mathbf{J}_{e_1}) - \frac{1}{4} g_{a\gamma\gamma} \vec{J}_{e_0} \cdot (\tilde{a}^* c \mathbf{B}_1 + \tilde{a} c \mathbf{B}_1^*) \\
&\left. - \frac{1}{4} (\mathbf{E}_1 \cdot \mathbf{J}_{e_1}^* + \mathbf{E}_1^* \cdot \mathbf{J}_{e_1}) \right) dV,
\end{aligned} \tag{64}$$

the same as eqn. (27) in the main text, and.

$$\begin{aligned}
\oint j \text{Im}(\mathbf{S}_{DB}) \cdot \hat{n} ds &= \int \left(\frac{j\omega_1}{2} \left(\frac{1}{\mu_0} \mathbf{B}_1^* \cdot \mathbf{B}_1 - \epsilon_0 \mathbf{E}_1 \cdot \mathbf{E}_1^* \right) \right. \\
&+ \frac{j(\omega_1 + \omega_a)}{4} \epsilon_0 g_{a\gamma\gamma} c \vec{B}_0 \cdot (\tilde{a} \mathbf{E}_1^* + \tilde{a}^* \mathbf{E}_1) + \\
&\frac{1}{4} g_{a\gamma\gamma} c \vec{B}_0 \cdot (\tilde{a} \mathbf{J}_{e_1}^* - \tilde{a}^* \mathbf{J}_{e_1}) + \frac{1}{4} g_{a\gamma\gamma} \vec{J}_{e_0} \cdot (\tilde{a}^* c \mathbf{B}_1 - \tilde{a} c \mathbf{B}_1^*) \\
&\left. - \frac{1}{4} (\mathbf{E}_1 \cdot \mathbf{J}_{e_1}^* - \mathbf{E}_1^* \cdot \mathbf{J}_{e_1}) \right) dV
\end{aligned} \tag{65}$$

the same as eqn. (28) in the main text

B. Axion Modified Abraham Poynting Theorem

To derive eqn. (31) and (32), we begin with writing the divergence of the real and imaginary part of \mathbf{S}_{EH} as,

$$\begin{aligned}
\nabla \cdot \text{Re}(\mathbf{S}_{EH}) &= \frac{1}{2} \nabla \cdot (\mathbf{S}_{EH} + \mathbf{S}_{EH}^*) \\
\nabla \cdot \text{Im}(\mathbf{S}_{EH}) &= \frac{1}{2} \nabla \cdot (\mathbf{S}_{EH} - \mathbf{S}_{EH}^*)
\end{aligned} \tag{66}$$

The next step is to calculate $\nabla \cdot \mathbf{S}_{EH}$ and $\nabla \cdot \mathbf{S}_{EH}^*$,

$$\begin{aligned}
\nabla \cdot \mathbf{S}_{EH} &= \frac{1}{2} \nabla \cdot (\mathbf{E}_1 \times \frac{1}{\mu_0} \mathbf{B}_1^*) = \\
&\frac{1}{2} \left(\frac{1}{\mu_0} \mathbf{B}_1^* \cdot \nabla \times \mathbf{E}_1 - \mathbf{E}_1 \cdot \frac{1}{\mu_0} \nabla \times \mathbf{B}_1^* \right),
\end{aligned} \tag{67}$$

and,

$$\begin{aligned}
\nabla \cdot \mathbf{S}_{EH}^* &= \frac{1}{2} \nabla \cdot (\mathbf{E}_1^* \times \frac{1}{\mu_0} \mathbf{B}_1) = \\
&\frac{1}{2} \left(\frac{1}{\mu_0} \mathbf{B}_1 \cdot \nabla \times \mathbf{E}_1^* - \mathbf{E}_1^* \cdot \frac{1}{\mu_0} \nabla \times \mathbf{B}_1 \right).
\end{aligned} \tag{68}$$

Considering the Abraham Poynting vector, under a background DC B-field of, $\vec{B}_0(\vec{r})$, created by an impressed electrical DC current in the magnet coil, \vec{J}_{e_0} , in harmonic form, Ampere's law is modified but Faraday's law is not, and may be written as,

$$\begin{aligned}
\frac{1}{\mu_0} \nabla \times \mathbf{B}_1 &= \mathbf{J}_{e_1} - j\omega_1 \epsilon_0 \mathbf{E}_1 + j\omega_a g_{a\gamma\gamma} \epsilon_0 c \vec{B}_0 \tilde{a} \\
\frac{1}{\mu_0} \nabla \times \mathbf{B}_1^* &= \mathbf{J}_{e_1}^* + j\omega_1 \epsilon_0 \mathbf{E}_1^* - j\omega_a g_{a\gamma\gamma} \epsilon_0 c \vec{B}_0 \tilde{a}^* \\
\nabla \times \mathbf{E}_1 &= j\omega_1 \mathbf{B}_1 \\
\nabla \times \mathbf{E}_1^* &= -j\omega_1 \mathbf{B}_1^*.
\end{aligned} \tag{69}$$

Substituting eqns. (69) into eqns. (67) and (68) leads to.

$$\begin{aligned}
\nabla \cdot \mathbf{S}_{EH} &= \frac{j\omega_1}{2} \left(\frac{1}{\mu_0} \mathbf{B}_1^* \cdot \mathbf{B}_1 - \epsilon_0 \mathbf{E}_1 \cdot \mathbf{E}_1^* \right) \\
&+ \frac{j\omega_a}{2} g_{a\gamma\gamma} \epsilon_0 \tilde{a}^* c \vec{B}_0 \cdot \mathbf{E}_1 - \frac{1}{2} \mathbf{E}_1 \cdot \mathbf{J}_{e_1}^*,
\end{aligned} \tag{70}$$

and,

$$\begin{aligned}
\nabla \cdot \mathbf{S}_{EH}^* &= \frac{j\omega_1}{2} \left(\epsilon_0 \mathbf{E}_1 \cdot \mathbf{E}_1^* - \frac{1}{\mu_0} \mathbf{B}_1^* \cdot \mathbf{B}_1 \right) \\
&- \frac{j\omega_a}{2} g_{a\gamma\gamma} \epsilon_0 \tilde{a} c \vec{B}_0 \cdot \mathbf{E}_1^* - \frac{1}{2} \mathbf{E}_1^* \cdot \mathbf{J}_{e_1}
\end{aligned} \tag{71}$$

Now by substituting (70) and (71) into (66) we obtain,

$$\begin{aligned}
\nabla \cdot \text{Re}(\mathbf{S}_{EH}) &= \frac{j\omega_a}{4} \epsilon_0 g_{a\gamma\gamma} c \vec{B}_0 \cdot (\tilde{a}^* \mathbf{E}_1 - \tilde{a} \mathbf{E}_1^*) \\
&- \frac{1}{4} (\mathbf{E}_1 \cdot \mathbf{J}_{e_1}^* + \mathbf{E}_1^* \cdot \mathbf{J}_{e_1}),
\end{aligned} \tag{72}$$

and

$$\begin{aligned} \nabla \cdot j \operatorname{Im}(\mathbf{S}_{EH}) &= \frac{j\omega_1}{2} \left(\frac{1}{\mu_0} \mathbf{B}_1^* \cdot \mathbf{B}_1 - \epsilon_0 \mathbf{E}_1 \cdot \mathbf{E}_1^* \right) \\ &+ \frac{j\omega_a}{4} \epsilon_0 g_{a\gamma\gamma} c \vec{B}_0 \cdot (\tilde{a}^* \mathbf{E}_1 + \tilde{a} \mathbf{E}_1^*) \\ &- \frac{1}{4} (\mathbf{E}_1 \cdot \mathbf{J}_{e_1}^* - \mathbf{E}_1^* \cdot \mathbf{J}_{e_1}) \end{aligned} \quad (73)$$

Then applying the divergence theorem, we arrive at,

$$\oint \operatorname{Re}(\mathbf{S}_{EH}) \cdot \hat{n} ds = \int \left(\frac{j\omega_a}{4} \epsilon_0 g_{a\gamma\gamma} c \vec{B}_0 \cdot (\tilde{a}^* \mathbf{E}_1 - \tilde{a} \mathbf{E}_1^*) \right. \\ \left. - \frac{1}{4} (\mathbf{E}_1 \cdot \mathbf{J}_{e_1}^* + \mathbf{E}_1^* \cdot \mathbf{J}_{e_1}) \right) dV \quad (74)$$

and the same as eqn. (31) in the main text, and.

$$\oint j \operatorname{Im}(\mathbf{S}_{EH}) \cdot \hat{n} ds = \int \left(\frac{j\omega_1}{2} \left(\frac{1}{\mu_0} \mathbf{B}_1^* \cdot \mathbf{B}_1 - \epsilon_0 \mathbf{E}_1 \cdot \mathbf{E}_1^* \right) \right. \\ \left. + \frac{j\omega_a}{4} \epsilon_0 g_{a\gamma\gamma} c \vec{B}_0 \cdot (\tilde{a}^* \mathbf{E}_1 + \tilde{a} \mathbf{E}_1^*) \right. \\ \left. - \frac{1}{4} (\mathbf{E}_1 \cdot \mathbf{J}_{e_1}^* - \mathbf{E}_1^* \cdot \mathbf{J}_{e_1}) \right) dV \quad (75)$$

the same as eqn. (32) in the main text

IX. Appendix B: Consideration of the Reactive Power Flow in a Resonant Haloscope

In this appendix we consider the impact of the reactive part of the Poynting vector on a resonant cavity axion haloscope. In general reactive coupling of power into a resonant cavity may be calculated by implementing Foster's reactance theorem [115, 116, 121]. Foster showed that a lossless circuit network made of resonances and anti-resonances could be represented as a combination of inductor's and capacitors[116] and following this Beringer and Dicke applied the theorem to high-Q microwave cavities[115, 121], allowing the calculation of the effect of reactive coupling to a cavity, based on the complex Poynting theorem [114]. In general, it has been shown that the reactive coupling network into a high-Q resonance may be either represented by an impedance, \mathcal{X}_1 in series with a parallel LC circuit (of elements L_{p1} , C_{p1} and R_{p1}), or an admittance, \mathcal{B}_1 , in parallel with a series LC circuit (of elements L_{s1} , C_{s1} and R_{s1}). Applying this technique to axion-photon conversion in a resonant haloscope, leads to the following equivalent circuit shown in Fig. 3.

Applying Foster's reactance theorem to the cavity resonator allows \mathcal{X}_1 and \mathcal{B}_1 to be calculated from the following equations [121],

$$j\mathcal{X}_1 = j\omega_1 \frac{4(U_{B1} - U_{E1})}{\tilde{I}\tilde{I}^*} \quad \text{and} \quad j\mathcal{B}_1 = j\omega_1 \frac{4(U_{E1} - U_{B1})}{\tilde{V}\tilde{V}^*}. \quad (76)$$

where

$$U_{B1} = \frac{1}{4\mu_0} \int \mathbf{B}_1^* \cdot \mathbf{B}_1 dV \quad \text{and} \quad U_{E1} = \frac{\epsilon_0}{4} \int \mathbf{E}_1 \cdot \mathbf{E}_1^* dV \quad (77)$$

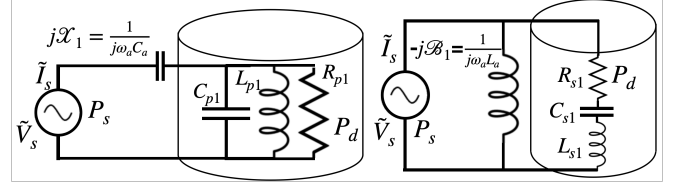


FIG. 3: Left, equivalent parallel LCR circuit representation of an axion coupling to a resonant cavity haloscope. Right, the equivalent series LCR circuit representation.

Following this procedure, the axion-photon coupling input impedances for both the axion modified Abraham Poynting Vector and the axion modified Minkowski Poynting Vector may be calculated, and is undertaken in the following sections.

1. Abraham Poynting Vector

To calculate the parameters for the parallel LCR circuit shown in fig.3, eqns.(76) and (32) are combined, and given that the real part of \mathbf{E}_1 is out of phase with any conduction currents in the volume, and zero at the cavity boundary, then the series impedance becomes,

$$j\mathcal{X}_1 = -j \frac{\omega_a \int \epsilon_0 g_{a\gamma\gamma} c \vec{B}_0 \cdot (\tilde{a}^* + \tilde{a}) \operatorname{Re}(\mathbf{E}_1) dV}{\tilde{I}\tilde{I}^*}. \quad (78)$$

Then given that the energy in a LC resonator is given by $U_1 = \frac{1}{2} \tilde{I}\tilde{I}^* L_{p1}$, where, $\omega_1^2 = \frac{1}{L_{p1} C_{p1}}$, and using the result from eqn. (37), eqn. (78) becomes,

$$j\mathcal{X}_1 = \frac{\omega_a}{j\omega_1^2 C_{p1}} \frac{\frac{a_0 \epsilon_0 g_{a\gamma\gamma} c}{2} \int \vec{B}_0 \cdot \operatorname{Re}(\mathbf{E}_1) dV}{U_1} = \frac{\omega_a}{j\omega_1^2 C_{p1}}, \quad (79)$$

which is equivalent to a capacitance of $C_a = C_{p1} \frac{\omega_1^2}{\omega_a^2}$. Thus, the input impedance, $Z_p(\omega_a)$ of the parallel circuit representation can be written in normalized form as,

$$\frac{Z_p(\omega_a)}{R_{p1}} = \frac{\omega_a}{j\omega_1 Q_1} + \frac{1}{1 + jQ_1 \left(\frac{\omega_a}{\omega_1} - \frac{\omega_1}{\omega_a} \right)}, \quad (80)$$

where $Q_1 = \omega_1 R_{p1} C_{p1}$. Defining the detuning as $\delta\omega = \omega_a - \omega_1$, where $\delta\omega \ll \omega_1$ and $\delta_a = \frac{\delta\omega}{\omega_1}$, then

$$\frac{Z_p(\delta_a)}{R_{p1}} \approx \frac{1 - j2Q_1(\delta_a + \frac{1}{2Q_1^2})}{1 + 4Q_1^2\delta_a^2}, \quad (81)$$

Setting the imaginary part to zero allows the calculation of the frequency shift of the resonant mode due to the axion coupling, which gives $\frac{\delta\omega_1}{\omega_1} \sim -\frac{1}{2Q_1^2}$ a very small frequency shift, which to first order does not affect the sensitivity of the axion haloscope and is the same order as a frequency shift due to dissipation. Ignoring this term gives the usual complex response of a resonant LCR circuit.

To calculate the parameters for the series *LCR* circuit shown in fig.3, we can use a similar procedure given $U_1 = \frac{1}{2}\tilde{\mathcal{V}}\tilde{\mathcal{V}}^*C_{s1}$, where, $\omega_1 = \frac{1}{L_{s1}C_{s1}}$, along with eqns. (76) and (32) to show that the parallel input admittance is given by,

$$-j\mathcal{B}_1 = \frac{\omega_a}{j\omega_1^2 L_{s1}} \frac{\frac{a_0\epsilon_0 g_{a\gamma\gamma} c}{2} \int \vec{B}_0 \cdot \text{Re}(\mathbf{E}_1) dV}{U_1} = \frac{\omega_a}{j\omega_1^2 L_{s1}}, \quad (82)$$

which is equivalent to an inductance of $L_a = L_{s1} \frac{\omega_1^2}{\omega_a^2}$. Thus, the input admittance, $Y_s(\omega_a)$, of the series circuit representation may be written in normalized form as,

$$R_{s1}Y_s(\omega_a) = \frac{\omega_a}{j\omega_1 Q_1} + \frac{1}{1 + jQ_1 \left(\frac{\omega_a}{\omega_1} - \frac{\omega_1}{\omega_a} \right)}, \quad (83)$$

where $Q_1 = \frac{\omega_1 L_{s1}}{R_{s1}}$, so

$$R_{s1}Y_s(\omega_a) \approx \frac{1 - j2Q_1(\delta_a + \frac{1}{2Q_1^2})}{1 + 4Q_1^2\delta_a^2}, \quad (84)$$

which completes the dual representation of the resonant axion haloscope as either a parallel *LCR* in series with a capacitive coupling element or a series *LCR* circuit in parallel with an inductive coupling element.

2. Minkowski Poynting Vector

The reactive part of the Minkowski Poynting vector as written in eqn. (28) has extra terms compared to the Abraham Poynting vector, and by following a similar process, the equivalent equation for the series impedance can be calculated to be,

$$j\mathcal{X}_{1M} = \frac{\omega_a + \omega_1}{j\omega_1^2 C_{p1}} \frac{\frac{\epsilon_0 g_{a\gamma\gamma} a_0 c}{2} \int \vec{B}_0 \cdot \text{Re}(\mathbf{E}_1) dV}{U_1} + \frac{1}{4\omega_1^2 C_{p1}} \frac{g_{a\gamma\gamma} c \int \vec{B}_0 \cdot (\tilde{a}^* \mathbf{J}_{e1} - \tilde{a} \mathbf{J}_{e1}^*) dV}{U_1} \quad (85)$$

The second term is non-zero due to lossless inductive currents at the cavity surface, κ_{e1} which are in phase with the magnetic field, \mathbf{B}_1 , and related by $\kappa_{e1} = \frac{1}{\mu_0} \hat{n} \times \mathbf{B}_1$,

where \hat{n} is the normal to the cavity surface, and because the surface current and magnetic field are in imaginary phase, then $\kappa_{e1}^* = -\kappa_{e1}$. Note $\mathbf{J}_{e1} = 0$, over the volume, unless there is loss in the volume, which contributes to the real part of the Poynting vector not the reactive part. Next, by implementing the identity, $\oint d\vec{s} \times \mathbf{B}_1 = \int \nabla \times \mathbf{B}_1 dV$, and from eqn. (18), to first order we may substitute the following, $\nabla \times \mathbf{B}_1 \rightarrow -j\omega_1 \epsilon_0 \mathbf{E}_1$ (ignoring terms second order in $g_{a\gamma\gamma}$). Then it is straightforward to show (given $d\vec{s} = ds\hat{n}$),

$$\begin{aligned} \vec{B}_0 \cdot \int (\tilde{a}^* \mathbf{J}_{e1} - \tilde{a} \mathbf{J}_{e1}^*) dV &= 2a_0 \vec{B}_0 \cdot \oint \kappa_1 ds \\ &= 2a_0 \vec{B}_0 \cdot \oint d\vec{s} \times \mathbf{B}_1 = -2ja_0 \omega_1 \int \vec{B}_0 \cdot \text{Re}(\mathbf{E}_1) dV, \end{aligned} \quad (86)$$

for the resonant cavity haloscope. Therefore substituting eqn. (86) into (85), the series impedance becomes,

$$j\mathcal{X}_{1M} = \frac{\omega_a + 2\omega_1}{j\omega_1^2 C_{p1}} \quad (87)$$

So the effective input capacitance represented in Fig.3 becomes, $C_a = C_{p1} \frac{\omega_1}{\omega_a(2 + \frac{\omega_a}{\omega_1})}$, which is about a factor of three smaller than C_a for the Abraham equivalent circuit when $\omega_a \sim \omega_1$. The normalised input impedance to first order in δ_a can thus be written as,

$$\frac{Z_p(\delta_a)}{R_{p1}} \approx \frac{1 - j2Q_1(\delta_a + \frac{3}{2Q_1^2})}{1 + 4Q_1^2\delta_a^2}, \quad (88)$$

Setting the imaginary part to zero allows the calculation of the frequency shift of the resonant mode due to the axion coupling, which gives $\frac{\delta\omega_1}{\omega_1} \sim -\frac{3}{2Q_1^2}$ a very small frequency shift but a factor of 3 greater than what the Abraham Poynting vector predicts. A precision frequency measurement of the axion interacting with a microwave cavity haloscope would be needed to determine this frequency shift.

A similar calculation can be undertaken for the effective parallel inductance for the series *LCR* circuit representation, the end result is an inductance of $L_a = L_{s1} \frac{\omega_1}{\omega_a(2 + \frac{\omega_a}{\omega_1})}$ leading to similar conclusions and a normalised input admittance of,

$$R_{s1}Y_s(\omega_a) \approx \frac{1 - j2Q_1(\delta_a + \frac{3}{2Q_1^2})}{1 + 4Q_1^2\delta_a^2}, \quad (89)$$

which completes our analysis.